Supporting Information for
Integrated, systems metabolic picture of acetone-butanol-ethanol fermentation by *Clostridium acetobutylicum*

Chen Liao, Seung-Oh Seo, Venhar Celik, Huaiwei Liu, Wentao Kong, Yi Wang
Hans Blaschek, Yong-Su Jin and Ting Lu

Contents

1 An integrated model for the ABE fermentation

The ABE fermentation of *C. acetobutylicum* is a complex, system-level process that involves the orchestration of metabolism, gene regulation and cell-environment interactions. Acknowledging the complexity of the process, we divided the underlying system into three functional modules, corresponding to metabolic reactions, gene regulation and environmental cues as shown in Fig. 1 in the main text. Subsequently, we constructed individual modules and characterized them in terms of their input-output relationship as well as dynamic properties. Afterwards, we assembled the modules into an integrated framework by connecting the output of one module to the input of another to form a closed loop. A system-level analysis was subsequently pursued to validate the integrated framework and also to illustrate its power in predicting ABE fermentation. Details of the model are presented below.

1.1 Metabolic reaction module

The metabolic reaction module describes the biochemical reactions associated with cellular central metabolism and the ABE fermentation. In this module, the concentration of Spo0A$\sim$P (the phosphorylated Spo0A) serves as the system input, owing to the fact that it controls the expression of the genes responsible for solvent formation. The outputs of this module are simply the concentrations of metabolic products. As the metabolite amounts in culture equal the sum of metabolites produced by individual cells, we described the kinetics of the overall metabolites by considering: the kinetics of metabolites within a single cell (Sec. 1.1.1), the availability and activity of enzymes involved in the metabolic reactions (Sec. 1.1.2), and the dynamics of population growth (Sec. 1.1.3).

1.1.1 Biochemical reactions

Fig. S1/S2 shows the biochemical reactions involved in the ABE fermentation, where the carbon source glucose is converted to acids and solvents in an ordered manner. In this diagram, we condensed all intermediate steps and complex regulations in glycolysis into a single reaction for pyruvate production. Pyruvate is then branched to enter the tricarboxylic acid (TCA) cycle (1), to lactate synthesis, or to produce acetyl-CoA. Acetyl-CoA is further branched to produce ethanol, acetate, or butyryl-CoA which is converted to butyrate or butanol. During the conversion from acetyl-CoA to butyryl-CoA, flux can also be divided to produce acetone. Additionally, the organic acids (acetate and butyrate) can be re-assimilated via a CtfAB-dependent pathway or putative reversed reactions to synthesize the corresponding solvents (acetone, butanol and ethanol). It is important to note that we introduced reverse reactions for Ack/Pta and Buk/Ptb as alternative pathways for acetate and butyrate re-utilizations respectively, supported by the previous literature (2, 3). Enzymes involved in these reactions are listed in the figure.

Mathematically, the biochemical reactions in Fig. S2 can be described in terms of their reaction rates (Tab. S1). Here, Michaelis-Menten kinetics was employed to model the enzymatic kinetics for all of the reactions but the CtfAB-dependent acid re-assimilations (r_{11} and r_{24}). In each of those kinetic processes, it involves two characteristic parameters: V, the maximal reaction rate at which substrate concentration is saturated, and K_m, the substrate concentration at which the reaction rate is equal to half of the maximum. For the CtfAB-dependent re-assimilations, a Ping-Pong-Bi-Bi mechanism was adopted to describe the sequential conversions of two substrates into two products catalyzed by a single enzyme (4). Therefore, the reactions r_{11} and r_{24} both have two K_m's. Additionally, acetoacetate and butanol were assumed to inhibit the enzymatic activities of CtfAB and AdhE$_1$ respectively, supported by the previous studies (4, 5).

The above descriptions of the biochemical reactions allow a quantitative modeling of the kinetics of all of the metabolites involved in the pathway. Here we employed ordinary differential equations to

describe the time evolution of these metabolites through the equations below (Eqs. S1-S17).

$$\frac{d[Pyr]}{dt} = \frac{2r_1}{V_c} - r_2 - r_3 - r_4 + r_5 \quad \text{(S1)}$$

$$\frac{d[Lactate]}{dt} = r_4 - r_5 \quad \text{(S2)}$$

$$\frac{d[AcCoA]}{dt} = r_3 + r_8 + r_{11} - r_7 - r_6 - r_{13} - r_{15} \quad \text{(S3)}$$

$$\frac{d[AcAcCoA]}{dt} = \frac{r_6}{2} - r_{11} - r_{24} - r_{17} \quad \text{(S4)}$$

$$\frac{d[AuP]}{dt} = r_7 + r_{10} - r_8 - r_9 \quad \text{(S5)}$$

$$\frac{d[Acetate]}{dt} = r_9 - r_{10} - r_{11} \quad \text{(S6)}$$

$$\frac{d[AcAc]}{dt} = r_{11} + r_{24} - r_{12} \quad \text{(S7)}$$

$$\frac{d[Acetone]}{dt} = r_{12} \quad \text{(S8)}$$

$$\frac{d[AcAld]}{dt} = r_{13} + r_{15} - r_{14} - r_{16} \quad \text{(S9)}$$

$$\frac{d[Ethanol]}{dt} = r_{14} + r_{16} \quad \text{(S10)}$$

$$\frac{d[3HBCoA]}{dt} = r_{17} - r_{18} \quad \text{(S11)}$$

$$\frac{d[CroCoA]}{dt} = r_{18} - r_{19} \quad \text{(S12)}$$

$$\frac{d[BuCoA]}{dt} = r_{19} + r_{21} + r_{24} - r_{20} - r_{25} \quad \text{(S13)}$$

$$\frac{d[BuP]}{dt} = r_{20} + r_{23} - r_{21} - r_{22} \quad \text{(S14)}$$

$$\frac{d[Butyrate]}{dt} = r_{22} - r_{23} - r_{24} \quad \text{(S15)}$$

$$\frac{d[BuAld]}{dt} = r_{25} - r_{26} \quad \text{(S16)}$$

$$\frac{d[Butanol]}{dt} = r_{26} \quad \text{(S17)}$$

Note that, the factors 2 in Eq. S1 and $1/2$ in Eq. S4 are due to stoichiometric constraints of the reactions. In addition, the single-cell glucose uptake rate r_1, which defines how fast the total amount (not the concentration) of glucose is imported into cells, needs to be scaled by the cell volume V_c (Eq. S1), when computing the intracellular concentration change.

1.1.2 Enzyme availability and activity

Due to their engagements in the reactions in Fig. S2, enzymes are essential in determining the actual rates of the biochemical reactions. To quantitatively model how enzymes impact ABE fermentation, we considered both their availability and activity. Here, enzyme availability refers to the abundance of an

enzyme, which can be quantified by its copy number, while enzyme activity refers to the catalytic activity of a single copy of an enzyme, which is often subject to the availability of external factors such as ATP, NADH, and other co-factors. To model enzyme availability, we classified the enzyme genes in Fig. S2 into two classes:

- Genes that are constitutively expressed (green), including *ldh*, *pfor*, *pta*, *ack*, *thl*, *adhE2*[†], *hbd*, *crt*, *bcd*, *ptb* and *buk*: We assumed that the concentrations of these enzymes remain constant (normalized to unit concentration) throughout the fermentation course, based on the experimental findings showing that the mRNA levels of those enzyme genes keep roughly the same during the course of fermentation (9).

- Genes that are relevant to solvent production (red), including *adc*, *ctfAB*, and *adhE1*: We assumed that the productions of this class of enzymes are subject to the availability of the master regulator Spo0A∼P (phosphorylated Spo0A) in a Hill-function-like form. The kinetics of the enzymes can then be described as:

$$\frac{d[Adc]}{dt} = r^0_{adc} + r_{adc}\frac{[S^*]^{n_{adc}}}{{K_{adc}}^{n_{adc}} + [S^*]^{n_{adc}}} - d_{adc}[Adc] \quad \text{(S18)}$$

$$\frac{d[CtfAB]}{dt} = r^0_{ctf} + r_{ctf}\frac{[S^*]^{n_{ctf}}}{{K_{ctf}}^{n_{ctf}} + [S^*]^{n_{ctf}}} - d_{ctf}[CtfAB] \quad \text{(S19)}$$

$$\frac{d[AdhE_1]}{dt} = r^0_{adhe} + r_{adhe}\frac{[S^*]^{n_{adhe}}}{{K_{adhe}}^{n_{adhe}} + [S^*]^{n_{adhe}}} - d_{adhe}[AdhE_1] \quad \text{(S20)}$$

  where $[S^*]$ represents the concentration of Spo0A∼P. For each of the above three equations, the first term corresponds to the basal enzyme production (rate constants: r^0_{adc}, r^0_{ctf} and r^0_{adhe}), the second corresponds to (Spo0A∼P)-activated enzyme production (rate constants: r_{adc}, r_{ctf} and r_{adhe}), and the last corresponds to first-order degradation (rate constants: d_{adc}, d_{ctf} and d_{adhe}).

To model enzyme activity, we assumed that there is a strong correlation between enzyme activity and cellular glucose uptake rate r_1. This assumption is built on the following two factors: (i) Several enzymes showed a diminishing activity when the glucose level in the medium reduces (10); (ii) The cofactors, such as ATP and NADH, that are important for catalytic reactions may have a limited availability when nutrient is limited (3). We therefore assumed that activities for all of the enzymes depend on the cellular glucose uptake in the following fashion: If the uptake rate is high, the activities for the enzymes remain intact. However, they drop when the imported glucose is not sufficient to provide the energy needed for a cell to maintain its basal-level metabolism. Computationally, we modeled the enzyme activity-glucose uptake relationship as:

$$\gamma = \begin{cases} 1 & \text{if } r_1 \geq \eta \\ (r_1/\eta)^{n_\gamma} & \text{otherwise} \end{cases} \quad \text{(S21)}$$

where γ is enzyme activity coefficient, r_1 is glucose uptake rate, η refers to the minimal energy needed for a cell to maintain its basal-level metabolism and n_γ reflects the nonlinearity of the relationship. The expressions of r_1 and η are detailed in Sec. 1.1.3.

[†]Despite of the fact that *adhE2* is highly induced in acidogenic phase and strongly repressed in solventogenic phase (6), we assumed a low yet constant level of this enzyme to account for the non-negligible background ethanol production in the *adhE1*-knockout strains (7, 8).

1.1.3 Glucose uptake and population growth

Glucose uptake: To model cellular growth, we built our model by first adopting the Monod equation widely used in describing cellular population dynamics (11). In addition, we incorporated into the model cellular growth inhibition that is originated from the toxicity of metabolites (such as butanol) produced by the cell and low pH (12, 13). Taken together, cellular glucose uptake rate r_1 can be written as

$$r_1 = \gamma \cdot \frac{V_1[Glu_e]}{K_{m1} + [Glu_e]}(1 - C_t) \tag{S22}$$

where Glu_e is the glucose in the medium (the subscript *e* refers to extracellular glucose) and C_t is a dimensionless metric describing the cellular toxicity level that is detailed in Sec. 1.3.1.

Specific growth rate: Recently, studies have shown that carbon sources imported by cells are not fully used for biomass synthesis and cellular growth, but instead, partially used to retain a basal-level metabolism (14, 15). Such a metabolism is needed even when cells do not grow and the associated minimal requirement is called maintenance cost (16). To model the total glucose consumption (ΔG) over a time interval of Δt, we partitioned it for cell growth and physiology maintenance, which can be described as

$$\Delta G = N_v r_1 \Delta t = \frac{\Delta B}{Y_G} + N_v \eta \Delta t \tag{S23}$$

where N_v is the number of viable cells (opposed to spores), ΔB is biomass production, Y_G is biomass yield and η is maintenance cost (η is assumed constant for simplicity). By assuming that biomass is proportional to cell number N_v, i.e.,

$$\Delta B = C_{biom} \Delta N_v \tag{S24}$$

where C_{biom} is the proportional coefficient and that cell population grows exponentially, i.e.,

$$\Delta N_v = \mu N_v \Delta t \tag{S25}$$

where μ is the specific growth rate, we were able to relate cellular growth rate μ to r_1 and η as

$$\mu = C_\mu (r_1 - \eta) \tag{S26}$$

in which $C_\mu = Y_G / C_{biom}$. Here, different from the typical nutrient–growth relationship, this equation naturally implies a negative growth rate (i.e., decreasing population number) when the amount of imported glucose is not sufficient to supply the minimal energy requirement for cell maintenance (17). It is worth pointing out that the mathematical definition of η includes two important processes contributing to a diversion of substrate flux from growth: (i) cell death and lysis and (ii) maintenance of plasmid replication.

Sporulation: One unique feature of *C. acetobutylicum* is its ability of spore formation in harsh environmental conditions, in addition to cellular apoptosis. We therefore partitioned the cell population into two subpopulations—viable cells and spores, and modeled them separately. For cellular transition from viable cells to spore, we assumed that it is triggered by cellular toxicity C_t, similar to the transition from acedogenic to solventogenic phases. In addition, as spore formation requires sequential activation of a large set of genes (18), it often involves a long time delay from cellular commitment to the completion of spore formation.

Taken together, we were able to derive the kinetic equations for external glucose (Glu_e), viable cell number (N_v), spore number (N_s), and optical density (OD_{600}) as follows

$$\frac{d[Glu_e]}{dt} = -\frac{N_v \cdot r_1}{V_m} \tag{S27}$$

$$\frac{dN_v}{dt} = C_\mu(r_1 - \eta)N_v - k_{spo} \cdot N_v(t - \delta_t) \cdot C_t(t - \delta_t) \tag{S28}$$

$$\frac{dN_s}{dt} = k_{spo} \cdot N_v(t - \delta_t) \cdot C_t(t - \delta_t) \tag{S29}$$

$$\frac{dOD_{600}}{dt} = \frac{C_{od,v}}{V_m}\frac{dN_v}{dt} + \frac{C_{od,s}}{V_m}\frac{dN_s}{dt} \tag{S30}$$

where V_m is the culture volume, k_{spo} is the maximum spore formation rate, δ_t is time delay for sporulation. Due to morphological distinctions between spores and non-spores, we used two light absorbance coefficients $C_{od,v}$ and $C_{od,s}$ for viable cells and spores respectively.

1.2 Gene regulation module

Although the importance of the master regulator Spo0A in regulating metabolic shift has been well elucidated (19), there has been lack of a system-level understanding about how cells utilize the underlying Spo0A-based network to integrate environmental signals and to implement cellular phase transitions.

Based on the previous experimental reports (18, 20, 21), we proposed a core regulatory network for cellular decision making in ABE fermentation. As shown in Fig. S3, the network centers on the master regulator Spo0A and its phosphorylated form Spo0A∼P, whose transitions are triggered by environmental signals, such as pH (22) and undissociated acids (23). In addition, the network contains a positive feedback loop mediated by two sigma factors σ^F and σ^K (20, 21). The intermediate sigma factors within the transcriptional cascade from σ^F to σ^K (e.g., σ^E, σ^G) are not modeled. Furthermore, the phosphorylated master regulator (Spo0A∼P) controls the expression of the downstream genes, including *adc*, *ctfAB*, and *adhE*, responsible for cellular transition from acidogenic to solventogenic phase. Therefore, in this module, environmental signals serve as the system input and Spo0A∼P serves as the output. It is important to notice that current understanding of the molecular details of the network is still incomplete and it is not our intent to develop a comprehensive model that includes every details of the network. Instead, we aimed to construct a kinetic model that is simple enough but yet captures the essential feature of the network. In particular, the model shall have the following characteristics: (i) the system has two stable states (acidogenesis and solventogenesis); (ii) there is positive feedback regulation; (iii) regulation involves a complex cascade consisting of multiple regulatory genes; and (iv) the system is capable of sensing the environmental cues and responding accordingly by driving the switch from one state to the other state.

To model how cells integrate multiple, complex environmental signals, such as undissociated acetate and butyrate, butanol, pH and other factors, we introduced a quantitative metric, cellular toxicity, as a measure of overall deleterious effects from the environment. Our rationale for the introduction of this metric is based on the fact that, from the perspective of cellular survival, the activation of Spo0A network is a consequence of toxicity-induced cellular stress response: The accumulation of undissociated acids, low pH, and other factors are toxic to cells and thereby cause cellular stress. As a strategy responding to these stresses, cells respond by shifting from acid production to solvent production for detoxification. This assumption is also consistent to the findings that, in addition to activating solvent-formation genes, Spo0A also serves as a master regulator of sporulation—an extraordinary protection mechanism for bacteria. Therefore, although the factors inducing cellular stress are diverse, their effects

are the same—to introduce toxicity and trigger cellular stress response. Therefore, the metric, cellular toxicity, can be used to unify all these signaling factors (detailed mathematical form of cellular toxicity is presented in Eq. S36).

More specifically, we assumed that cellular toxicity regulates the availability of the kinase responsible for Spo0A phosphorylation and, by responding to cellular toxicity, the rate of phosphorylation will increase, which can be mathematically expressed as

$$F(C_t) = \frac{(C_t/K_t)^{n_t}}{1 + (C_t/K_t)^{n_t}} \tag{S31}$$

where $F(C_t)$ is the kinase activity which varies between zero and one depending on the toxicity level C_t. K_t and n_t are dissociation constant and Hill coefficient respectively. In this model, BuP (24) was not taken into account for solventogenesis regulation, owing to controversies on its role (2).

A mathematical model describing the entire gene regulation of ABE fermentation can then be described as

$$\frac{d[S]}{dt} = (\alpha_{S0} + \alpha_S \frac{[SigK]^{n_S}}{K_S^{n_S} + [SigK]^{n_S}}) - \beta_K \gamma F(C_t) \frac{[S]}{Q_S^K + [S]} + \beta_P \gamma \frac{[S^*]}{Q_{S^*}^P + [S^*]} - d_S[S] \tag{S32}$$

$$\frac{d[S^*]}{dt} = \beta_K \gamma F(C_t) \frac{[S]}{Q_S^K + [S]} - \beta_P \gamma \frac{[S^*]}{Q_{S^*}^P + [S^*]} - d_{S^*}[S^*] \tag{S33}$$

$$\frac{d[SigF]}{dt} = (\alpha_{F0} + \alpha_F \frac{[S^*]^{n_F}}{K_F^{n_F} + [S^*]^{n_F}}) - d_F[SigF] \tag{S34}$$

$$\frac{d[SigK]}{dt} = (\alpha_{K0} + \alpha_K \frac{[SigF]^{n_K}}{K_K^{n_K} + [SigF]^{n_K}}) - d_K[SigK] \tag{S35}$$

where S, S^*, $SigF$ and $SigK$ are the concentrations of Spo0A, Spo0A∼P, σ^F and σ^K, respectively. Here, The productions of Spo0A, σ^F and σ^K consist of two parts, one basal rate ($\alpha_{S0},\ \alpha_{F0},\ \alpha_{K0}$) and the other Hill-function-like production term ($\alpha_S,\ \alpha_F,\ \alpha_K$ are the maximal rates, $K_S,\ K_F,\ K_K$ are the dissociation constants, and $n_S,\ n_F,\ n_K$ are the Hill coefficients). Additionally, all of the species follow a first-order degradation with rate constants as d_S, d_{S*}, d_F and d_K for Spo0A, Spo0A∼P, σ^F and σ^K correspondingly. Furthermore, the phosphorylation of Spo0A is modeled using a Michaelis-Menten equation (the maximal rate β_K and dissociation constant Q_S) multiplied by the cellular toxicity function $F(C_t)$ to reflect the fact that Spo0A phosphorylation is subject to environmental toxicity. In contrast, dephosphorylation is modeled using standard Michaelis-Menten equation alone (maximal rate β_P and dissociation constant Q_{S^*}).

1.3 Environmental cues module

The metabolic and gene regulatory networks constitute the major infrastructures for cellular processes in the ABE fermentation. They mutually impact each other through the mediation of environmental cues (Fig. S4). For instance, molecules produced from metabolic reactions are released to intracellular compartment and then to extracellular milieu through diffusion, causing the change of environmental status such as pH; conversely, the molecular composites in the environment, including undissociated acids and protons (pH), can be toxic to the cells and thereby induce cellular stress response through the alteration of gene expression. Here we developed a mathematical framework for quantitative modeling of environmental cues by addressing the following issues: cellular toxicity (Sec. 1.3.1), acid dissociation (Sec. 1.3.2), metabolite diffusion (Sec. 1.3.3), and external and internal pH (Sec. 1.3.4).

1.3.1 Cellular toxicity

We first introduced a unified metric, cellular toxicity, to account for the overall effects of environmental cues to cellular physiology. This is due to the following facts (12, 13, 25–27) (discussion is also available in the third paragraph of Sec 1.2): (i) A subset of metabolites, such as organic acids and solvents, are shown toxic to the cells; (ii) a high level of these molecules can reduce and even fully inhibit cellular growth; and (iii) the solvent production of *C. acetobutylicum* is a cellular survival strategy responding to environmental stress.

We further proposed that cell toxicity is a function of butanol, undissociated acids, and intracellular pH. Here, we only considered butanol but not acetone or ethanol, owing to the fact that the toxicity of acetone and ethanol is negligible compared to that of acetate and butyrate (13). In addition, we modeled the undissociated but not dissociated forms of the acids because of the evidence showing that undissociated acids are more toxic (8, 28, 29). Based on the previous work (13), the quantitative expression of cellular toxicity can be expressed as

$$\begin{aligned} C_t &= \left(\frac{[Acetate_i^u]}{Z_{aa}}\right)^{m_{aa}} + \left(\frac{[Butyrate_i^u]}{Z_{ba}}\right)^{m_{ba}} + \left(\frac{[Butanol_i]}{Z_b}\right)^{m_b} \\ &+ m_1 \left(\frac{[Acetate_i^u]}{Z_{aa}}\right)^{m_{aa}} \left(\frac{[Butanol_i]}{Z_b}\right)^{m_b} \\ &+ m_2 \left(\frac{[Butyrate_i^u]}{Z_{ba}}\right)^{m_{ba}} \left(\frac{[Butanol_i]}{Z_b}\right)^{m_b} \\ &+ m_3 \left(\frac{[Acetate_i^u]}{Z_{aa}}\right)^{m_{aa}} \left(\frac{[Butyrate_i^u]}{Z_{ba}}\right)^{m_{ba}} \\ &+ m_{pH} \left(\theta_{pH} - pH_i\right) \Theta \left(\theta_{pH} - pH_i\right) \end{aligned} \tag{S36}$$

where the subscript *i* indicates intracellular metabolite and the superscript *u* indicates undissociated acid. Additionally, Z_x ($x = aa, ba, b$ for acetate, butyrate and butanol, respectively) is the coefficient reflecting the inhibitory threshold of the metabolites, m_x ($x = aa, ba, b$) reflects the inhibition cooperativity, and m_1, m_2 and m_3 are the coefficients for the synergistic effects between acids and butanol, observed experimentally (13). The step-function Θ is used here to reflect the fact that pH contributes to cellular toxicity only if it is below a threshold value θ_{pH}.

To enable the calculation of cellular toxicity proposed above, we subsequently developed three sets of equations to account for acid association, metabolite diffusion, and pH change.

1.3.2 Acid dissociation

Due to the fact that acid dissociation reaches equilibrium at a much faster time scale compared with those of gene expression and enzymatic reactions, we assumed that dissociation equilibrium is always satisfied in our system. The corresponding acid dissociation processes can then be described using the Henderson-Hasselbalch equation as

$$[A_{i,j}^u] = \frac{[A_{i,j}^t]}{1 + 10^{pH_i - pK_{a,j}}} \tag{S37}$$

$$[A_{e,j}^u] = \frac{[A_{e,j}^t]}{1 + 10^{pH_e - pK_{a,j}}} \tag{S38}$$

where $A_{m,j}^n$ is a dissociable acid, with j refers to the type of acids (e.g., acetic acid, butyric acid and lactic acid); $m = \{i, e\}$ indicates whether the acid is intracellular or extracellular, and $n = \{u, d, t\}$ indicates

whether it is undissociated, dissociated, or total (undissociated plus dissociated acids). In addition, pH_i and pH_e are internal and external pH values respectively. $pK_{a,j}$ is the logarithmic equivalence of the acid dissociation constant $K_{a,j}$, i.e.,

$$pK_{a,j} = -\log_{10} K_{a,j} \tag{S39}$$

1.3.3 Metabolite diffusion

To model metabolite diffusion and equilibrium across cell membrane, we classified the metabolites associated with the ABE fermentation into two classes: general metabolites and dissociable acids. For general metabolites, we assumed that they diffuse across cell membrane with its rate proportional to the gradient of intra- and extra-cellular concentration, i.e.,

$$d_M = P \cdot ([M_i] - [M_e]) \tag{S40}$$

where $[M_i]$ and $[M_e]$ are the internal and external concentrations of the metabolite M, and P is the diffusion constant that characterizes how fast metabolite achieves equilibrium across cell membrane. For dissociable acids, we assumed that only the undissociated (not dissociated) forms of the acids can diffuse across cell membrane (22). The corresponding acid diffusion can be written as

$$d_A = P \cdot ([A_i^u] - [A_e^u]) \tag{S41}$$

where $[A_i^u]$ and $[A_e^u]$ are internal and external undissociated acid concentrations respectively.

The above assumptions allow us to model the partition of undissociated acids and other metabolites between intra- and extra-cellular environments as

$$\frac{d[X_i]}{dt} = \frac{d[X]}{dt} - d_X \tag{S42}$$

$$\frac{d[X_e]}{dt} = V_r \cdot d_X \tag{S43}$$

where $[X_i]$ and $[X_e]$ are the internal and external concentrations of any given metabolite X (M or A) respectively. The factor V_r is the the volume ratio of total viable cells (cell number N_v multiplied by the volume of an individual cell V_c) to the culture volume (V_m), i.e.,

$$V_r = \left(\frac{N_v}{V_m}\right) \cdot V_c \tag{S44}$$

Note that V_r is proportional to cell density and they differ by a factor of V_c.

To examine the intra- and extra-cellular equilibrium kinetics of the metabolites (Eq. S42 and Eq. S43), we simulated a set of metabolite equilibrium processes by setting up different initial concentrations of acetic acid, butyric acid and butanol for both inside and outside of the cells. The results are shown in Fig. S5 (panel A, B, C, E, F, G). As expected, butanol always achieves a final equal concentration across cell membrane while, for acetic and butyric acids, only their undissociated forms, instead of the total acids, have equal concentrations at equilibrium. To further illustrate how cell density impacts the outcomes of metabolite diffusion, we plotted in Fig. S6A the steady-state metabolite distribution as a function of V_r.

1.3.4 Extra- and intra-cellular pH

Extracellular pH: External pH (pH_e) is determined by considering both buffer composition and acidic metabolites released to environment by the cells. Here we proposed to use the charge-balance equation (30) to calculate environmental pH for any given medium composition. Since the culture medium is neutral, the net quantity of charges carried by acids, bases and buffers must be zero at equilibrium, leading to a general charge balance equation as (30, 31)

$$\sum_{Acids} C_A \frac{\sum_{i=1}^{M+1}\left\{(m+1-i)([H_e^+])^{i-1}\Pi_{j=1}^{j=M+1-i}K_{aj}\right\}}{\sum_{i=1}^{M+1}\left\{([H_e^+])^{i-1}\Pi_{j=1}^{j=M+1-i}K_{aj}\right\}} - \sum_{Bases} C_B \frac{\sum_{i=1}^{M+1}\left\{(m+1-i)([H_e^+])^{i-1}\Pi_{j=1}^{j=M+1-i}K_{bj}\right\}}{\sum_{i=1}^{M+1}\left\{([H_e^+])^{i-1}\Pi_{j=1}^{j=M+1-i}K_{bj}\right\}} + \frac{K_w}{[H_e^+]} - [H_e^+] - \sum_{Counterions} C_C \sum_{k=1}^{n_c} z_k = 0 \tag{S45}$$

where $[H_e^+]$ is environmental proton concentration which can be related to extracellular pH through the relation

$$pH_e = -\log_{10}[H_e^+] \tag{S46}$$

. In Eq. S45, C_A, C_B and C_C are the concentrations of acids, bases and counterions (e.g., K^+ and Cl^-) respectively, n_c is the number of counterions, z_k is the signed charge of a counterion, M is the number of dissociable sites, m equals M for acids and 0 for bases, and K_{aj}, K_{bj} and K_w are the equilibrium constants for acids, bases, and water respectively.

To illustrate the power of the above equation, we used it to compute the pH values of simple buffer solutions in Fig. S7, showing a great agreement with experimental reports over a wide range of chemical ingredients.

To further illustrate whether the same approach is applicable to complex culture media, we tested for the case of MS-MES medium whose buffer ingredients are listed in Tab. S7. Compared to the original compositions in (32), we neglected (i) $MgSO_4$ and $FeSO_4$, because they are nearly neutral, and (ii) p-aminobenzooic acid, biotin and resazurin, due to their low amounts. The charge balance equation for MS-MES medium can be expressed as

$$[Lactate_e^t]\frac{K_{la}}{K_{la}+[H_e^+]} + [Acetate_e^t]\frac{K_{aa}}{K_{aa}+[H_e^+]} + [Butyrate_e^t]\frac{K_{ba}}{K_{ba}+[H_e^+]} + (C_{kh_2po_4}+C_{k_2hpo_4})\frac{K_{p1}[H_e^+]^2+2K_{p1}K_{p2}[H_e^+]+3K_{p1}K_{p2}K_{p3}}{[H_e^+]^3+K_{p1}[H_e^+]^2+K_{p1}K_{p2}[H_e^+]+K_{p1}K_{p2}K_{p3}} + C_{mes}\frac{K_{mes}}{K_{mes}+[H_e^+]} - C_{nh_3}\frac{[H_e^+]}{K_{nh_3}+[H_e^+]} + \frac{K_w}{[H_e^+]} - [H_e^+] - (C_{kh_2po_4}+2C_{k_2hpo_4}) = 0 \tag{S47}$$

where $[Lactate_e^t]$, $[Acetate_e^t]$ and $[Butyrate_e^t]$ are total extracellular concentrations of lactate, acetate, and butyrate accordingly, and $[H_e^+]$ is environmental proton concentration. $C_{kh_2po_4}$, $C_{k_2hpo_4}$, C_{mes} and C_{nh3} are the external concentrations of KH_2PO_4, K_2HPO_4, MES, and ammonium solution respectively. K_{la}, K_{aa}, K_{ba}, K_{mes}, K_{nh3} are the dissociation constants of lactic acid, acetic acid, butyric acid, MES

and ammonia (converted from its base dissociation constant) respectively. Since phosphoric acid can dissociate up to three times, there are three acid dissociation constants, named K_{p1}, K_{p2} and K_{p3} here. The dissociation constant of water is K_w. Note that, in this model, we only considered the metabolites associated with the ABE fermentation but not the acids or bases from other metabolic events. In addition, ion exchanges between environment and cells through ion pumps were not modeled either.

Intracellular pH: For intracellular pH, its calculation is much more challenging because cells tend to maintain a relatively steady pH gradient across cell membrane via active proton transport instead of pure diffusion (22, 33, 34). Acknowledging this complexity, we proposed an empirical relationship between the intra- and extra-cellular pH by leveraging the fact that there is a steady pH gradient across cell membrane (22, 33)

$$pH_i = pH_e + \exp(a + b \cdot pH_e) \tag{S48}$$

where a and b are parameters (see Fig. S9) fit using the experimental data (33).

To demonstrate the feasibility of pH calculation, we employed the Eq. S47 and Eq. S48 for a few test cases in Fig. 2 (panel F and G) in the main text, Fig. S5 (panel D and H) and Fig. S6B.

2 Computational methods, parameters and initial conditions

2.1 Computational methods

Custom-tailored Matlab codes were developed to perform computational simulations of the ABE fermentation for various conditions and strains. The detailed implementations of the in silico experiments are described below:

Module development

Fig. 2A: The simulated profiles were obtained by solving Eqs. S1-S17, S18-S20 and S27-S30. Two typical Spo0A∼P concentration ($[S^*]$) patterns were used, with one inactivated throughout the time course and the other being activated during the course (step-function like). The cellular toxicity C_t was assumed to be proportional to Spo0A∼P, i.e., $C_t = (6.0 \times 10^{-4}) \cdot [S^*]$. An initial condition of 60 g/L glucose, 0.2 optical density and 0.2 L medium volume was used.

Fig. 2B-E: The bifurcation diagram (Fig. 2B) and cellular responses to cellular toxicity (Fig. 2C-E) were obtained by finding the roots of Eqs. S32-S35 at given values for the parameters scanned. In Fig. 2B, we scanned Spo0A production rate α_S and phosphatase activity of Spo0A dephosphorylation β_P while setting cellular toxicity C_t to 0.2. In Fig. 2C, we fixed β_P and scanned both α_S and C_t. The enzyme activity coefficient γ was set unit throughout the figure.

Fig. 2F-H: The external pH (Fig. 2F) was computed by solving Eq. S46-S47 for given acetic acid and butyric acid levels. The corresponding internal pH (Fig. 2G) was calculated through Eq. S48. Additionally, we computed cellular toxicity C_t via Eq. S36 using the measured experimental values of acetic acid, butyric acid and butanol concentrations at different time points of an ABE fermentation and plotted the evolution of cellular toxicity in Fig. 2H (wild type and *adc*-deficient strains data from (32)).

Module integration and model perturbations

Individual modules were assembled into an integrated model by combining the differential equations Eqs. S1-S17, S18-S20, S27-S30, S32-S35 and S42-S43 with the algebraic equations Eqs. S36, S37-S38, S45, S46 and S48. Computational simulations for the fermentation of the wild type *C. acetobutylicum* ATCC 824 strain were implemented by numerically integrating the above equations, along with the parameters detailed in Tab. S3-S6.

To create in silico knockout strains, we simply set null, in our model, for the production rate or the concentration of the proteins encoded by the target genes. For instance, the production rates of Adc (r_{adc}) and CtfAB (r_{ctf}) were separately set zero for the fermentations of *adc*- and *ctfA*-mutants in Fig. 3. Similarly, for *pta-ctfB-adhE1* triple knockout strain (Fig. 4 and Fig. S10), the Pta concentration ($[Pta]$), CtfAB production rate (r_{ctf}) and AdhE$_1$ production rate (r_{adhe}) were set zero. For *spo0A* knockout strain (Fig. 5), we set the Spo0A production rate (α_S) zero. Different from *spo0A* knockout, for *spo0A* overexpression fermentation (Fig. 5), we assigned seven copies to *spo0A* gene (35) in Eq. S32, which is mathematically equivalent to increase the maximal Spo0A production rate α_S by a factor of 6. Simultaneously, we increased cellular maintenance cost rate η to 8.0×10^{-9} for both control and *spo0A*-overexpression strains to mimic the metabolic burden caused by plasmid maintenance.

To implement in silico pH control, we discarded the calculated extracellular pH values through Eq. S45. Instead, we directly assigned a desired value to the variable of the extracellular pH when needed. For instance, for the fermentations with pH controlled above 5.0, we directly assigned a value of 5.0 to external pH pH_e when calculated extracellular pH from Eq. S45 drops below 5.0.

2.2 Parameters

The model parameters were obtained primarily through previous literature reports and our own data fitting. Most of the Michaelis constants K_m and the parameters regarding the gene expression of Spo0A network were acquired from the literature (4) and (36) accordingly. For those unavailable in literature, we employed two strategies, local and global optimizations, to search for appropriate parameter values. The parameters used in this study are all listed in Tab. S3-S6, with those from literature marked with special symbols.

Estimation of the diffusion constant P:

The Fick's law states that the diffusive flux (the amount of substance change per unit area per unit time) is $J = -D\frac{\partial c}{\partial r}$, where c is concentration of diffusive molecule, r is cell radius, and D is diffusion constant. Therefore, the total flux across the cell surface area can be rewritten as

$$J^c_{tot} = -\frac{4\pi r^2 D}{\frac{4}{3}\pi r^3}\frac{c_i - c_e}{r} = -\frac{3D}{r^2}(c_i - c_e) \tag{S49}$$

where c_i and c_e are intracellular and extracellular concentrations of the molecule of interest. By comparing this expression with the diffusion equation $dc_i/dt = -P(c_i - c_e)$, we can obtain an estimate of the diffusion constant $P \simeq 1.08 \times 10^7$ hr^{-1}, where we assumed $D \simeq 1.0 \times 10^{-5}$ cm^2·s^{-1} (typical for small molecule) and $r \simeq 1$ μm (typical for bacteria).

2.3 Initial conditions

The overview of initial conditions of all fermentations is available at Tab. S8. We chose the initial conditions, including glucose concentration, optical density and medium volume, that are consistent with reported experiments. An initial 0.02 optical density was used when OD_{600} data is unavailable form literature.

The concentrations of extracellular acids and solvents were always chosen to be the same as experimental descriptions. For the initial conditions of the intracellular acids and solvents, we assumed that the concentrations of intracellular undissociated (not total) acids equal to those of their extracellular counterparts and that intracellular and extracellular solvents have the same concentrations. For all other metabolites, both their internal and external concentrations were set as zero.

The initial intra- and extra-cellular pH values were always computed using Eq. S45 and Eq. S48 respectively, depending on both buffer compositions (Tab. S7) and initial acid concentrations in the environment. In addition, the initial cell number was chosen based on the initial OD_{600} from experiment, i.e.,

$$N_v(t=0) = \frac{V_m \cdot OD_{600}(t=0)}{C_{od,v}} \tag{S50}$$

$$N_s(t=0) = 0 \tag{S51}$$

We noticed that there may exist a lag phase at the beginning of fermentation in some reported experiments (e.g. the fermentations of wild-type strains in Fig. 3): During an initial period, there is neither glucose consumption nor cellular growth. To mimic the growth delay for a better model-experiment comparison, we computationally set r_1 to r_{26} to be zero for a certain amount of time (see the column of Delay in Tab. S8 for the values of the delays) before the model being normally integrated.

3 Model extension: cofactor balance

Cofactors, such as NAD(P)H/NAD(P)$^+$ and ATP/ADP, are generally important to cellular metabolic reactions. However, it has been shown that, for the case of clostridial ABE fermentation, the variations of NAD(P)H/NAD(P)$^+$ pools are comparable or smaller than their means and the fluctuations of ATP/ADP pools are even smaller (37), indicating that cells have intrinsic mechanisms to maintain their energy and redox homeostasis. In our original model described above, the framework is mathematically equivalent to the case where cofactors are assumed constants (see Sec. 3.1) and is further introduced with a global system parameter γ to reflect the overall state of a cell. Furthermore, our model has produced consistent results that agree well with experimental reports. Therefore, for this specific ABE fermentation system, constant cofactor approximations along with a global system parameter is a reasonable assumption. As a matter of fact, this assumption has also been adopted by previous computational models (38–40).

However, the impacts of cofactors can be exaggerated in some scenarios, particularly when the balances are significantly perturbed (41). To investigate this issue, in this section, we extended our model to incorporate cofactor kinetics and their modulation to metabolic reactions, and further used the extended model to conduct a case study. The details of the model extension and case study are shown below.

3.1 Mathematical model

Multi-substrate reactions: When considering energy or redox cofactors, metabolic reactions often involve two or more substrates, which can be generally classified as ping-pong or sequential mechanisms (42). To model such processes, here we assumed that enzyme-cofactor interactions follow a sequential mechanism where all substrates must bind to the enzyme before products can be released. We also assumed that different substrates bind to the enzyme in a random manner. Therefore, a triple-substrate reaction, the random sequential mechanism can be schematically described in Fig. S13.

The synthesis rate of product P can then be derived as

$$\nu_P = \frac{k_{cat}^A \cdot [E_T] \cdot \frac{[S]}{K_S} \cdot \frac{[A]}{K_{SA}} + k_{cat}^B \cdot [E_T] \cdot \frac{[S]}{K_S} \cdot \frac{[B]}{K_{SB}}}{1 + \frac{[S]}{K_S} + \frac{[A]}{K_F} + \frac{[B]}{K_B} + \frac{[S]}{K_S} \cdot \left(\frac{[A]}{K_{SA}} + \frac{[B]}{K_{SB}} \right)} \tag{S52}$$

where $[E_T]$ is the total enzyme level, $[S]$ is the substrate concentration, and $[A]$ and $[B]$ are the concentrations of two alternative cofactors. By assuming $k_{cat}^A = k_{cat}^B = k_{cat}$, $K_F = K_{SA}$ and $K_B = K_{SB}$, the above rate can be reduced to

$$\nu_P = \frac{V_{max}[S]}{K_S + [S]} \cdot \frac{\frac{[A]}{K_A} + \frac{[B]}{K_B}}{1 + \frac{[A]}{K_A} + \frac{[B]}{K_B}} \tag{S53}$$

where $V_{max} = k_{cat}[E_T]$. From this expression, we can find that the rate (Eq. S53) can be reduced to standard Michaelis-Menten equations when cofactor levels are either held constant or much larger than the corresponding dissociation constants (e.g., $[A] \gg K_F$, $[B] \gg K_B$). This conclusion can be generalized to other multi-substrate interaction mechanisms, such as ordered sequential mechanism and ping-pong mechanism, allowing us to extend the original model to incorporate cofactors.

Redox balance: By using the expression Eq. S53, we extended our original model to consider redox balance with detailed reactions listed in Tab. S9. Notably, six cofactor-dependent reactions were modified

compared to those in the original model (Eq. S3, Eq. S9, Eq. S10, Eq. S13, Eq. S16, and Eq. S17):

$$\frac{d[AcCoA]}{dt} = r_3 + r_8 + r_{11} - r_7 - r_6 - r_{13}^a - r_{13}^b - r_{15}^a - r_{15}^b \quad \text{(S54)}$$

$$\frac{d[AcAld]}{dt} = r_{13}^a + r_{13}^b + r_{15}^a + r_{15}^b - r_{14}^a - r_{14}^b - r_{16}^a - r_{16}^b \quad \text{(S55)}$$

$$\frac{d[Ethanol]}{dt} = r_{14}^a + r_{14}^b + r_{16}^a + r_{16}^b \quad \text{(S56)}$$

$$\frac{d[BuCoA]}{dt} = r_{19} + r_{21} + r_{24} - r_{20} - r_{25}^a - r_{25}^b \quad \text{(S57)}$$

$$\frac{d[BuAld]}{dt} = r_{25}^a + r_{25}^b - r_{26}^a - r_{26}^b \quad \text{(S58)}$$

$$\frac{d[Butanol]}{dt} = r_{26}^a + r_{26}^b \quad \text{(S59)}$$

In addition, we introduced differential equations to describe redox pairs, i.e., NADH/NAD^+, NADPH/$NADP^+$ and oxidized/reduced-ferredoxin, as follows

$$\frac{d[NADH]}{dt} = \frac{2r_1}{V_c} - r_4 + r_5 - r_{13}^a - r_{14}^a - r_{15}^a - r_{16}^a - r_{17} - r_{19} - r_{25}^a - r_{26}^a + r_{27} - r_{28} - r_{31}^a + r_{32}^a \quad \text{(S60)}$$

$$\frac{d[NAD^+]}{dt} = -\frac{d[NADH]}{dt} \quad \text{(S61)}$$

$$\frac{d[NADPH]}{dt} = -r_{13}^b - r_{14}^b - r_{15}^b - r_{16}^b - r_{25}^b - r_{26}^b + r_{29} - r_{30} - r_{31}^b + r_{32}^b \quad \text{(S62)}$$

$$\frac{d[NADP^+]}{dt} = -\frac{d[NADPH]}{dt} \quad \text{(S63)}$$

$$\frac{d[Fd^{ox}]}{dt} = -r_3 - r_{31}^a - r_{31}^b + r_{32}^a + r_{32}^b + r_{33} \quad \text{(S64)}$$

$$\frac{d[Fd^{red}]}{dt} = -\frac{d[Fd^{ox}]}{dt} \quad \text{(S65)}$$

where we assumed that the total concentrations of the oxidized and reduced forms of the each redox pair remain constant (43, 44). Here, additional electron transfers between NADH and NAD^+ that are not directly involved in the ABE fermentation pathway were modeled through the reversible reactions r_{27} and r_{28}. Similarly, the reactions r_{29} and r_{30} were used to describe the conversion between NADPH and $NADP^+$ in reactions other than those in the ABE pathways.

Experimental reports have shown that the metabolic enzymes Nfor (NAD(P)H-ferredoxin oxidoreductase), Fnr (ferredoxin-$NAD(P)^+$ reductase) and Hyd (hydrogenase) are differentially expressed: Nfor and Hyd are only active in acid-producing culture while Fnr has a higher specific activity in the solventogenic phase (4, 29). Although the detailed regulatory mechanism of these enzymes is unclear, the above experimental findings allow us to assume that these enzymes are indirectly regulated by the phorsphorylated

Spo0A, i.e.,

$$\frac{d[Nfor]}{dt} = r^0_{nfor} + r_{nfor}\frac{K^{n_{nfor}}_{nfor}}{K^{n_{nfor}}_{nfor} + [S^*]^{n_{nfor}}} - d_{nfor}[Nfor] \quad \text{(S66)}$$

$$\frac{d[Fnr]}{dt} = r^0_{fnr} + r_{fnr}\frac{[S^*]^{n_{fnr}}}{K^{n_{fnr}}_{fnr} + [S^*]^{n_{fnr}}} - d_{fnr}[Fnr] \quad \text{(S67)}$$

$$\frac{d[Hyd]}{dt} = r^0_{hyd} + r_{hyd}\frac{K^{n_{hyd}}_{hyd}}{K^{n_{hyd}}_{hyd} + [S^*]^{n_{hyd}}} - d_{hyd}[Hyd] \quad \text{(S68)}$$

The redox sensing protein, Rex, helps maintain redox balance by altering the gene expression of metabolic enzymes as a response to cellular redox status (45, 46). Free Rex proteins are the transcriptional repressors of many metabolic enzymes including those in the *bcs* operon and AdhE$_2$. NAD$^+$ binds to Rex as an effector that slightly increases the binding affinity of Rex to DNA sequence; by contrast, the binding of the reducing equivalent NADH significantly lowers its affinity. Meanwhile, there is no experimental evidence showing that Rex is NADPH-dependent (45). Here we assumed that the fraction of active Rex proteins (both free Rex proteins and NAD$^+$-bound Rex proteins) follows a Hill function of NADH/NAD$^+$ ratio, i.e.,

$$[Rex_a] = \frac{[Rex_t]}{1 + (R_x/K_x)^{n_x}} \quad \text{(S69)}$$

$$R_x = \frac{[NADH]}{[NAD^+]} \quad \text{(S70)}$$

where the total and active Rex protein concentrations are given by $[Rex_t]$ and $[Rex_a]$ respectively. Here, K_x describes the sensitivity of Rex protein to R_x (the NADH/NAD$^+$ ratio) and n_x is the Hill coefficient.

In *C. acetobutylicum*, Rex was reported† to repress *thl*, *hbd*, *crt*, *bcd*, *ptb*, *buk* and *adhE$_2$* (46). For each gene j, we assumed that, for each of the promoters, free Rex proteins and NAD$^+$-bound Rex proteins have the same corresponding binding affinity. Therefore, the Rex-dependent enzyme expression levels $[ENZ_j]$ are linearly proportional to their transcription rates controlled by the Rex protein concentration, which can be modeled as

$$[ENZ_j] \to [ENZ_j]\frac{W^{max}_j}{1 + \left(\frac{1}{K_{d,j}} \cdot \frac{[Rex_t]}{1 + (R_x/K_x)^{n_x}}\right)^{n_j}} \quad \text{(S71)}$$

where W^{max}_j, $K_{d,j}$ and n_j are the maximal upregulation of enzyme level $[ENZ_j]$, dissociation constant, and Hill coefficient respectively. Therefore, the kinetic rate of reaction k involving the enzyme $[ENZ_j]$ can be expressed as

$$r_k \to r_k\frac{W^{max}_j}{1 + \left(\frac{1}{K_{d,j}} \cdot \frac{[Rex_t]}{1 + (R_x/K_x)^{n_x}}\right)^{n_j}} \quad \text{(S72)}$$

Energy balance: The energy dependence of the reactions involved in the ABE pathways can be similarly modeled by substituting the single-substrate Michaelis-Menten kinetics with Eq. S53 (Here ATP/ADP

†Despite *ldh* gene holds a Rex-binding site and its transcript level increases greatly in *rex*-deficient strain, there was no significant change of lactate production compared to the wild-type fermentation (45), indicating the regulation may be complex on post-transcriptional level. As a consequence, we assumed the expression level of *ldh* is constitutive and Rex-independent.

are cofactors). For simplicity, for the case study discussed in the subsection below, we assumed constant levels of ATP and ADP throughout the entire course of fermentation. Our assumption is supported by two facts: (i) ATP/ADP variations are much smaller than those of redox during the wild-type *C. acetobutylicum* metabolism (37); (ii) For the case below, unlike the rebox balancing mechanism that was mutated, the intrinsic ATP/ADP balancing mechanism remains intact.

3.2 Case study: Rex-deficient strain as an ethanol producer

To illustrate the impacts of cofactors on the ABE fermentation in extreme scenarios, we performed two *in silico* fermentation assays with one using the wildtype and the other using a mutant strain whose the Rex gene is knocked out. Computationally, the later case was implemented by setting $[Rex_t]$ to zero in Eq. S72 for all of the Rex-dependent reactions.

As shown in Fig. S14, our computational fermentation results agree well with a previous experimental report (45). Interestingly, for the *rex* mutant, *adhE2* gene was highly overexpressed (de-repressed), leading to a significant increase of ethanol production and decrease of acetone production. This case study demonstrates our appropriate model extension and also shows that, in certain extreme cases, cofactors indeed play essential roles in the ABE fermentation.

Initial conditions The initial conditions of Fig. S14 are given in Tab. S8. Besides, the initial concentrations of NADH, NAD^+, NADPH, $NADP^+$ are 0.2 mM, 1.6 mM, 0.16 mM and 0.01 mM, respectively. All of these initial values are within the experimentally reported regions (1, 37). The ATP and ADP levels are, respectively, fixed at 10.0 mM and 2.0 mM which correspond to their maximum physiological values (1). The initial concentrations of oxidized and reduced ferredoxins are arbitrarily taken as 16.5 mM and 0 mM, respectively.

Parameters For this study, we kept the same values for the old parameters listed in Tab. S3-S6. For new parameters introduced in this section, we estimated their values if they are not available in literature

- The maximal catalytic rates 'V' (V_{27}-V_{30} have unit mM·hr^{-1} and V_{31}-V_{33} have unit hr^{-1}): $V_{27} = 5.0 \times 10^6$, $V_{28} = 3.9 \times 10^6$, $V_{29} = 4.0 \times 10^6$, $V_{30} = 5.0 \times 10^4$, $V_{31} = 1.0 \times 10^{10}$, $V_{32} = 1.0 \times 10^{10}$ and $V_{33} = 5.0 \times 10^{10}$;
- The Michaelis constants 'K' (unit: mM): $K_{r1} = 2.3 \times 10^{-1}$, $K_{e1} = 1.0 \times 10^{-1}$, $K_{e2} = 3.7 \times 10^{-1}$, $K_{f3} = 2.9 \times 10^{-2}$, $K_{r4} = 1.1 \times 10^{-2}$, $K_{r5} = 2.3 \times 10^{-1}$, $K_{e9} = 7.1 \times 10^{-1}$, $K_{e10} = 3.7 \times 10^{-1}$, $K^a_{r13} = 8.2 \times 10^{-3}$, $K^b_{r13} = 2.6 \times 10^{-1}$, $K^a_{r14} = 8.2 \times 10^{-3}$, $K^b_{r14} = 2.6 \times 10^{-1}$, $K^a_{r15} = 8.2 \times 10^{-3}$, $K^b_{r15} = 2.6 \times 10^{-1}$, $K^a_{r16} = 8.2 \times 10^{-3}$, $K^b_{r16} = 2.6 \times 10^{-1}$, $K_{r17} = 8.6 \times 10^{-3}$, $K_{r19} = 8.6 \times 10^{-3}$, $K_{e22} = 7.1 \times 10^{-1}$, $K_{e23} = 1.4$, $K^a_{r25} = 3.0 \times 10^{-3}$, $K^b_{r25} = 4.0 \times 10^{-2}$, $K^a_{r26} = 1.8 \times 10^{-1}$, $K^b_{r26} = 4.0 \times 10^{-2}$, $K_{r27} = 3.0 \times 10^{-1}$, $K_{r28} = 1.0 \times 10^{-2}$, $K_{r29} = 2.0$, $K_{r30} = 4.0 \times 10^{-2}$, $K_{f31} = 2.9 \times 10^{-2}$, $K^a_{r31} = 3.0 \times 10^{-3}$, $K^b_{r31} = 4.0 \times 10^{-2}$, $K_{f32} = 3.3 \times 10^{-3}$, $K^a_{r32} = 2.3 \times 10^{-1}$, $K^b_{r32} = 2.0$, $K_{f33} = 3.3 \times 10^{-3}$;
- Others: $r^0_{fnr} = 0.0$ mM·hr^{-1}, $r_{fnr} = 1.0 \times 10^2$ mM·hr^{-1}, $d_{fnr} = 7.2$ hr^{-1}, $K_{fnr} = 5.0 \times 10^2$ mM, $n_{fnr} = 2.0$, $r^0_{nfor} = 0.0$ mM·hr^{-1}, $r_{nfor} = 1.0 \times 10^2$ mM·hr^{-1}, $d_{nfor} = 7.2$ hr^{-1}, $K_{nfor} = 5.0 \times 10^2$ mM, $n_{fnor} = 2.0$, $r^0_{hyd} = 0.0$ mM·hr^{-1}, $r_{hyd} = 1.0 \times 10^4$ mM·hr^{-1}, $d_{hyd} = 7.2$ hr^{-1}, $K_{hyd} = 5.0 \times 10^2$ mM, $n_{hyd} = 2.0$, $n_x = 1.0$, $K_x = 1.0 \times 10^{-2}$, $W^{max}_{thl} = 3.2$, $[Rex_t]/K_{d,thl} = 3.0 \times 10^1$, $n_{thl} = 1.0$, $W^{max}_{adhE_2} = 3.8 \times 10^1$, $[Rex_t]/K_{d,adhE_2} = 5.0 \times 10^2$, $n_{adhE_2} = 1.0$, $W^{max}_{hbd} = 3.2$, $[Rex_t]/K_{d,hbd} = 3.0 \times 10^1$, $n_{hbd} = 1.0$, $W^{max}_{crt} = 3.2$, $[Rex_t]/K_{d,crt} = 3.0 \times 10^1$, $n_{crt} = 1.0$, $W^{max}_{bcd} = 3.2$, $[Rex_t]/K_{d,bcd} = 3.0 \times 10^1$, $n_{bcd} = 1.0$, $W^{max}_{ptb} = 6.9$, $[Rex_t]/K_{d,ptb} = 8.0 \times 10^1$, $n_{ptb} = 1.0$, $W^{max}_{buk} = 2.1$, $[Rex_t]/K_{d,thl} = 1.5 \times 10^1$, $n_{buk} = 1.0$.

4 Materials and experimental methods

Bacteria strains and media: The wild-type *C. acetobutylicum* ATCC 824 spore lab stock was heat-shocked at 80°C for 10 min, followed by cooling on ice for 5 min. The heat-shocked spores were inoculated at a 1% inoculum level into in tryptone-glucose-yeast extract (TGY) medium containing 30 g/L tryptone, 20 g/L glucose, 10 g/L yeast extract and 1 g/L L-cysteine. The TGY culture was incubated at 37°C for 12-14 h in an anaerobic chamber under N_2:CO_2:H_2 (volume ratio of 85:10:5) atmosphere. The growing culture was inoculated into MS-MES medium in BioFlo® 115 benchtop bioreactors (New Brunswick Scientific Co., Enfield, CT) at a 5% inoculum level. The MS-MES medium used in this study contained the following compounds: 0.55 g/L KH_2PO_4; 0.55 g/L K_2HPO_4; 0.22 g/L $MgSO_4{\cdot}7H_2O$; 0.011 g/L $FeSO_4{\cdot}7H_2O$; 2.3 ml/L acetic acid; 0.01 g/L NaCl; 40 μg/L p-aminobenzoic acid; 0.32 μg/L biotin; 1 mg/L resazurin; 21.3 g/L 2-(N-morpholino) ethane-sulfonic acid (MES). High purity nitrogen was purged through the medium until the OD_{600} of culture was reached at 1.0 which makes media under anaerobic condition by own gas productions, CO_2 and H_2. Temperature was controlled at 37°C and agitation was carried out at 55 rpm. Cell growth and fermentation products were monitored throughout the course of fermentation. The pH profiles of each fermentations were recorded using the NBS BioCommand® software (New Brunswick Scientific Co., Enfield, CT).

Analytical techniques: Analysis of cell growth and fermentation products. Cell growth was measured by optical density (O.D.) in the fermentation broth at A_{600} using a BioMate3 Spectrophotometer (Thermo, New York, USA). Acetone, butanol, ethanol, acetate and butyrate were measured and quantified by high performance liquid chromatography (HPLC) (Agilent Technologies 1200 Series) system equipped with a refractive index (RI) detector using Biorad Aminex HPX-87H column (300 x 7.8 mm). The column was eluted with 0.005 N of H_2SO_4 at a flow rate of 0.6 mL/min at 30°C.

5 Supplementary Tables

Reaction	Kinetic Law	Reaction	Kinetic Law
Glu → 2 Pyr	$r_1 = \gamma \cdot \frac{V_1[Glu_e]}{K_{m1} + [Glu_e]} \cdot (1 - C_t)$	Pyr → (TCA cycle)	$r_2 = \gamma \cdot \frac{V_2[Pyr_i]}{K_{m2} + [Pyr_i]}$
Pyr → AcCoA	$r_3 = \gamma \cdot [Pfor] \cdot \frac{V_3[Pyr_i]}{K_{m3} + [Pyr_i]}$	Pyr → Lactate	$r_4 = \gamma \cdot [Ldh] \cdot \frac{V_4[Pyr_i]}{K_{m4} + [Pyr_i]}$
Lactate → Pyr	$r_5 = \gamma \cdot [Ldh] \cdot \frac{V_5[Lactate_i^t]}{K_{m5} + [Lactate_i^t]}$	2 AcCoA → AcAcCoA	$r_6 = \gamma \cdot [Thl] \cdot \frac{V_6[AcCoA_i]}{K_{m6} + [AcCoA_i]}$
AcCoA → AcP	$r_7 = \gamma \cdot [Pta] \cdot \frac{V_7[AcCoA_i]}{K_{m7} + [AcCoA_i]}$	AcP → AcCoA	$r_8 = \gamma \cdot [Pta] \cdot \frac{V_8[AcP_i]}{K_{m8} + [AcP_i]}$
AcP → Acetate	$r_9 = \gamma \cdot [Ack] \cdot \frac{V_9[AcP_i]}{K_{m9} + [AcP_i]}$	Acetate → AcP	$r_{10} = \gamma \cdot [Ack] \cdot \frac{V_{10}[Acetate_i^t]}{K_{m10} + [Acetate_i^t]}$
Acetate + AcAcCoA → AcCoA + AcAc		$r_{11} = \gamma \cdot [CtfAB] \cdot \frac{V_{11}}{1 + \frac{K_{m11a}}{[Acetate_i^t]} + \frac{K_{m11b}}{[AcAcCoA_i]}} \cdot \frac{1}{1 + \frac{[AcAc_i]}{K_{i11}}}$	
AcAc → Acetone	$r_{12} = \gamma \cdot [Adc] \cdot \frac{V_{12}[AcAc_i]}{K_{m12} + [AcAc_i]}$	AcCoA → AcAld	$r_{13} = \gamma \cdot [AdhE_1] \cdot \frac{V_{13}[AcCoA_i]}{K_{m13} + [AcCoA_i]}$
AcAld → Ethanol	$r_{14} = \gamma \cdot [AdhE_1] \cdot \frac{V_{14}[AcAld_i]}{K_{m14} + [AcAld_i]}$	AcCoA → AcAld	$r_{15} = \gamma \cdot [AdhE_2] \cdot \frac{V_{15}[AcCoA_i]}{K_{m15} + [AcCoA_i]}$
AcAld → Ethanol	$r_{16} = \gamma \cdot [AdhE_2] \cdot \frac{V_{16}[AcAld_i]}{K_{m16} + [AcAld_i]}$	AcAcCoA → 3HBCoA	$r_{17} = \gamma \cdot [Hbd] \cdot \frac{V_{17}[AcAcCoA_i]}{K_{m17} + [AcAcCoA_i]}$
3HBCoA → CroCoA	$r_{18} = \gamma \cdot [Crt] \cdot \frac{V_{18}[3HBCoA_i]}{K_{m18} + [3HBCoA_i]}$	CroCoA → BuCoA	$r_{19} = \gamma \cdot [Bcd] \cdot \frac{V_{19}[CroCoA_i]}{K_{m19} + [CroCoA_i]}$
BuCoA → BuP	$r_{20} = \gamma \cdot [Ptb] \cdot \frac{V_{20}[BuCoA_i]}{K_{m20} + [BuCoA_i]}$	BuP → BuCoA	$r_{21} = \gamma \cdot [Ptb] \cdot \frac{V_{21}[BuP_i]}{K_{m21} + [BuP_i]}$
BuP → Butyrate	$r_{22} = \gamma \cdot [Buk] \cdot \frac{V_{22}[BuP_i]}{K_{m22} + [BuP_i]}$	Butyrate → BuP	$r_{23} = \gamma \cdot [Buk] \cdot \frac{V_{23}[Butyrate_i^t]}{K_{m23} + [Butyrate_i^t]}$
Butyrate+ AcAcCoA → BuCoA + AcAc		$r_{24} = \gamma \cdot [CtfAB] \cdot \frac{V_{24}}{1 + \frac{K_{m24a}}{[Butyrate_i^t]} + \frac{K_{m24b}}{[AcAcCoA_i]}} \cdot \frac{1}{1 + \frac{[AcAc_i]}{K_{i24}}}$	
BuCoA → BuAld		$r_{25} = \gamma \cdot [AdhE_1] \cdot \frac{V_{25}[BuCoA_i]}{K_{m25} + [BuCoA_i]}$	
BuAld → Butanol		$r_{26} = \gamma \cdot [AdhE_1] \cdot \frac{V_{26}[BuAld_i]}{K_{m26} + [BuAld_i](1 + \frac{[Butanol_i]}{K_{i26}})}$	

Table S1: Kinetic laws of the primary metabolic reactions described in Fig. S2.

Metabolite	Kinetic Law	Metabolite	Kinetic Law
Pyr	$d_{Pyr} = P \cdot ([Pyr_i] - [Pyr_e])$	AcCoA	$d_{AcCoA} = P \cdot ([AcCoA_i] - [AcCoA_e])$
AcAcCoA	$d_{AcAcCoA} = P \cdot ([AcAcCoA_i] - [AcAcCoA_e])$	AcP	$d_{AcP} = P \cdot ([AcP_i] - [AcP_e])$
Acetate	$d_{Acetate} = P \cdot ([Acetate_i^u] - [Acetate_e^u])$	AcAc	$d_{AcAc} = P \cdot ([AcAc_i] - [AcAc_e])$
Acetone	$d_{Acetone} = P \cdot ([Acetone_i] - [Acetone_e])$	AcAld	$d_{AcAld} = P \cdot ([AcAld_i] - [AcAld_e])$
Ethanol	$d_{Ethanol} = P \cdot ([Ethanol_i] - [Ethanol_e])$	3HBCoA	$d_{3HBCoA} = P \cdot ([3HBCoA_i] - [3HBCoA_e])$
CroCoA	$d_{CroCoA} = P \cdot ([CroCoA_i] - [CroCoA_e])$	BuCoA	$d_{BuCoA} = P \cdot ([BuCoA_i] - [BuCoA_e])$
BuP	$d_{BuP} = P \cdot ([BuP_i] - [BuP_e])$	Butyrate	$d_{Butyrate} = P \cdot ([Butyrate_i^u] - [Butyrate_e^u])$
BuAld	$d_{BuAld} = P \cdot ([BuAld_i] - [BuAld_e])$	Butanol	$d_{Butanol} = P \cdot ([Butanol_i] - [Butanol_e])$
Lactate	$d_{Lactate} = P \cdot ([Lactate_i^u] - [Lactate_e^u])$		

Table S2: Kinetic laws of free diffusion of reactive metabolites through cell membrane (Sec. 1.3.3). The **u**ndissociated acids are labeled using superscript u. P is diffusion constant across membrane.

Parameter	Value	Parameter	Value	Parameter	Value
K_{la}	1.38×10^{-4}	K_{aa}	1.74×10^{-5}	K_{ba}	1.51×10^{-5}
K_{p1}	7.08×10^{-3}	K_{p2}	6.92×10^{-8}	K_{p3}	4.68×10^{-13}
K_{mes}	1.05×10^{-6}	K_{nh3}	5.62×10^{-10}	K_w	1.00×10^{-14}

Table S3: The acid dissociation constants (K_a) of the buffers in Tab. S7.

Parameter	Value	Parameter	Value	Parameter	Value	Parameter	Value
V_1	1.4×10^{-8}	V_2	5.0×10^{5}	V_3	8.0×10^{6}	V_4	2.5×10^{5}
V_5	2.0×10^{5}	V_6	5.6×10^{6}	V_7	1.0×10^{6}	V_8	2.0×10^{5}
V_9	8.5×10^{7}	V_{10}	6.0×10^{6}	V_{11}	4.2×10^{10}	V_{12}	1.0×10^{11}
V_{13}	2.4×10^{8}	V_{14}	2.0×10^{9}	V_{15}	1.2×10^{5}	V_{16}	4.2×10^{4}
V_{17}	7.0×10^{6}	V_{18}	3.0×10^{7}	V_{19}	5.0×10^{6}	V_{20}	1.0×10^{8}
V_{21}	4.0×10^{8}	V_{22}	8.0×10^{6}	V_{23}	8.5×10^{4}	V_{24}	3.0×10^{10}
V_{25}	5.0×10^{13}	V_{26}	5.0×10^{13}				

Table S4: The maximal catalytic rates 'V'. The units for all of the rates are hr^{-1} except V_1 and V_2 which have the units $mmol \cdot hr^{-1}$ and $mM \cdot hr^{-1}$ respectively.

Parameter	Value	Parameter	Value	Parameter	Value	Parameter	Value
$K_{m1}^{(*)}$	4.6×10^{1}	K_{m2}	5.0×10^{-2}	$K_{m3}^{(\dagger)}$	3.2×10^{-1}	$K_{m4}^{(\ddagger)}$	6.0×10^{-2}
$K_{m5}^{(\ddagger)}$	2.5×10^{1}	$K_{m6}^{(\dagger)}$	2.8×10^{-1}	$K_{m7}^{(\dagger)}$	2.1×10^{-1}	K_{m8}	1.1×10^{-1}
$K_{m9}^{(\dagger)}$	5.8×10^{-1}	$K_{m10}^{(\dagger)}$	7.3×10^{1}	$K_{m11a}^{(\dagger)}$	1.2×10^{3}	$K_{m11b}^{(\dagger)}$	2.1×10^{-2}
$K_{m12}^{(\dagger)}$	8.2	$K_{m13}^{(\dagger)}$	1.5×10^{-1}	$K_{m14}^{(\ddagger)}$	3.9×10^{-1}	K_{m15}	1.5×10^{-1}
K_{m16}	3.9×10^{-1}	$K_{m17}^{(\dagger)}$	1.4×10^{-2}	$K_{m18}^{(\dagger)}$	3.0×10^{-2}	K_{m19}	2.5×10^{-3}
$K_{m20}^{(\dagger)}$	1.1×10^{-1}	$K_{m21}^{(\dagger)}$	2.6×10^{-1}	K_{m22}	4.7×10^{-1}	$K_{m23}^{(\dagger)}$	1.4×10^{1}
$K_{m24a}^{(\dagger)}$	6.6×10^{2}	$K_{m24b}^{(\dagger)}$	5.6×10^{-2}	$K_{m25}^{(\dagger)}$	4.5×10^{-2}	$K_{m26}^{(\dagger)}$	1.6×10^{1}
K_{i11}	2.0×10^{-1}	K_{i24}	2.0×10^{-1}	$K_{i26}^{(\dagger)}$	2.1×10^{2}		

$^{(*)}$ (3).

$^{(\dagger)}$ (4).

$^{(\ddagger)}$ (47).

Table S5: The Michaelis constants 'K_m' and 'K_i'. Unit: mM.

Category	Parameter	Value	Unit	Parameter	Value	Unit
Growth	$V_c^{(*)}$	4.2×10^{-15}	L	$C_{od,v}$	3.1×10^{-9}	
	$C_{od,s}$	3.1×10^{-9}		C_μ	1.8×10^{7}	mmol^{-1}
	η	2.8×10^{-9}	mmol·hr^{-1}	n_γ	5.0×10^{-1}	
	$k_{spo}^{(\dagger)}$	9.0×10^{-3}	hr^{-1}	$\delta_t^{(\ddagger)}$	1.0×10^{1}	hr
Toxicity$^{(\S)}$	Z_{aa}	6.0×10^{1}	mM	m_{aa}	1.5	
	Z_{ba}	9.0×10^{1}	mM	m_{ba}	1.5	
	Z_b	2.3×10^{2}	mM	m_b	2.0	
	m_1	1.0		m_2	1.0	
	m_3	0.0		m_{pH}	5.0×10^{-1}	
	θ_{pH}	6.18				
Spo0A	α_{S0}	7.2×10^{-1}	nM·hr^{-1}	α_S	7.2×10^{2}	nM·hr^{-1}
	K_S	1.0×10^{2}	nM	n_S	1.5	
	β_K	3.6×10^{4}	nM·hr^{-1}	β_P	1.8×10^{1}	nM·hr^{-1}
	Q_S^K	1.0×10^{4}	nM	Q_{S*}^P	1.0×10^{1}	nM
	$d_S^{(\P)}$	7.2	hr^{-1}	$d_{S*}^{(\P)}$	3.6×10^{-2}	hr^{-1}
	α_{F0}	7.2×10^{-1}	nM·hr^{-1}	$\alpha_F^{(\P)}$	1.4×10^{3}	nM·hr^{-1}
	K_F	2.3×10^{3}	nM	$n_F^{(\P)}$	1.0	
	$d_F^{(\P)}$	7.2	hr^{-1}	α_{K0}	1.2×10^{2}	nM·hr^{-1}
	$\alpha_K^{(\P)}$	1.4×10^{3}	nM·hr^{-1}	$K_K^{(\P)}$	2.0×10^{1}	nM
	$n_K^{(\P)}$	1.0		$d_K^{(\P)}$	7.2	hr^{-1}
	n_t	4.0		K_t	0.3	
Enzyme	r_{adc}^0	2.0×10^{1}	nM·hr^{-1}	r_{adc}	5.2×10^{3}	nM·hr^{-1}
	${d_{adc}}^{(\P)}$	7.2	hr^{-1}	K_{adc}	5.0×10^{2}	nM
	n_{adc}	2.0		r_{ctf}^0	0.0	nM·hr^{-1}
	r_{ctf}	1.5×10^{3}	nM·hr^{-1}	${d_{ctf}}^{(\P)}$	7.2	hr^{-1}
	K_{ctf}	5.0×10^{2}	nM	n_{adc}	2.0	
	r_{adhe}^0	0.0	nM·hr^{-1}	r_{adhe}	1.0×10^{4}	nM·hr^{-1}
	${d_{adhe}}^{(\P)}$	7.2	hr^{-1}	K_{adhe}	1.0×10^{3}	nM
	n_{adhe}	2.0				
Others	a	4.1		b	-8.2×10^{-1}	
	P	1.1×10^{7}	hr^{-1}			

$^{(*)}$ Cell volume is estimated based on the assumption that cells are spherical with a radius 1 μm.

$^{(\dagger)}$ (48).

$^{(\ddagger)}$ (35).

$^{(\S)}$ (13).

$^{(\P)}$ (36).

Table S6: Additional parameters used in the simulations.

Medium	KH_2PO_4	K_2HPO_4	NH_4Ac	$(NH_4)_2SO_4$	MES	$NH_3 \cdot H_2O$	HAc
CGM	0.75	0.75	0.00	2.00	0.00	0.00	0.00
SCM	0.50	0.38	2.20	0.00	0.00	0.00	0.00
MS-MES	0.55	0.55	0.00	0.00	7.99	1.12	0.00
MS-MES w/ acetate	0.55	0.55	0.00	0.00	7.99	1.12 2.22	2.30

Table S7: Compositions of the culture media used in this study (unit: g/L). For fermentations using MS-MES medium supplemented with acetate, either 1.12 or 2.22 g/L ammonium solution was used depending on the reported initial pH value.

Figure	Strain	pH-control	Medium(*)	Glucose (g/L)	OD_{600}	Volume (L)	Delay (hr)	Ref
3A	wild type	No	MS-MES	60.0	0.22	0.2	8.0	(32)
	adc$^-$				0.18			
	ctfA$^-$				0.14		0.0	
3B	wild type	No	MS-MES w/ acetate	60.0	0.20	1.5	9.0	this study
							0.0	
					0.12	0.2	0.0	(45)
					0.02			(49)
4B	*pta*$^-$, *ctfB*$^-$, *adhE*$_1^-$	pH ≥ 5.0	CGM	100.0	0.14	2.0	0.0	(8)
5	wild type	pH ≥ 5.0	CGM	80.0	0.02	0.4	0.0	(50)
	spo0A$^-$							
	wild type (empty plasmid)							(51)
	spo0A overexpression							
6	wild type	pH ≥ 5.0	MS-MES w/ acetate	60.0	0.43	1.3	0.0	(2)
		pH ≥ 5.5			0.50		7.2	
		pH ≥ 6.0	SCM	55.0	0.02	2.0	0.0	(52)
S10	*pta*$^-$, *ctfB*$^-$, *adhE*$_1^-$	pH ≥ 6.0	CGM	100.0	0.30	2.0	0.0	(8)
S11	wild type	pH ≥ 5.0	SCM	55.0	0.02	2.0	0.0	(52)
			CGM	80.0	0.04	5.0		(19)
				100.0	0.22	2.0		(53)
			MS-MES w/ acetate	60.0	0.43	1.3		(2)
S14	wild type	No	MS-MES w/ acetate	60.0	0.12	0.2	0.0	(45)
	rex$^-$							

(*) See Tab. S7 for concentrations of buffer components.

Table S8: Summary of experiment-specific parameters used in the simulations.

Reaction	Kinetic Law
Glu + 2 ADP + 2 NAD^+ → 2 Pyr + 2 ATP + 2 NADH	$r_1 = \gamma \cdot \frac{V_1[Glu_e]}{K_{m1} + [Glu_e]} \cdot \frac{[ADP]}{K_{e1} + [ADP]} \cdot \frac{[NAD^+]}{K_{r1} + [NAD^+]} \cdot (1 - C_t)$
Pyr + ATP → (TCA cycle) + ADP	$r_2 = \gamma \cdot \frac{V_2[Pyr_i]}{K_{m2} + [Pyr_i]} \cdot \frac{[ATP]}{K_{e2} + [ATP]}$
Pyr + Fd^{ox} → AcCoA + Fd^{red}	$r_3 = \gamma \cdot [Pfor] \cdot \frac{V_3[Pyr_i]}{K_{m3} + [Pyr_i]} \cdot \frac{[Fd^{ox}]}{K_{f3} + [Fd^{ox}]}$
Pyr + NADH → Lactate + NAD^+	$r_4 = \gamma \cdot [Ldh] \cdot \frac{V_4[Pyr_i]}{K_{m4} + [Pyr_i]} \cdot \frac{[NADH]}{K_{r4} + [NADH]}$
Lactate + NAD^+ → Pyr + NADH	$r_5 = \gamma \cdot [Ldh] \cdot \frac{V_5[Lactate_i^t]}{K_{m5} + [Lactate_i^t]} \cdot \frac{[NAD^+]}{K_{r5} + [NAD^+]}$
2 AcCoA → AcAcCoA	$r_6 = \gamma \cdot [Thl] \cdot \frac{V_6[AcCoA_i]}{K_{m6} + [AcCoA_i]}$
AcCoA → AcP	$r_7 = \gamma \cdot [Pta] \cdot \frac{V_7[AcCoA_i]}{K_{m7} + [AcCoA_i]}$
AcP → AcCoA	$r_8 = \gamma \cdot [Pta] \cdot \frac{V_8[AcP_i]}{K_{m8} + [AcP_i]}$
AcP + ADP → Acetate + ATP	$r_9 = \gamma \cdot [Ack] \cdot \frac{V_9[AcP_i]}{K_{m9} + [AcP_i]} \cdot \frac{[ADP]}{K_{e9} + [ADP]}$
Acetate + ATP → AcP + ADP	$r_{10} = \gamma \cdot [Ack] \cdot \frac{V_{10}[Acetate_i^t]}{K_{m10} + [Acetate_i^t]} \cdot \frac{[ATP]}{K_{e10} + [ATP]}$
Acetate + AcAcCoA → AcCoA + AcAc	$r_{11} = \gamma \cdot [CtfAB] \cdot \frac{V_{11}}{1 + \frac{K_{m11a}}{[Acetate_i^t]} + \frac{K_{m11b}}{[AcAcCoA_i]}} \cdot \frac{1}{1 + \frac{[AcAc_i]}{K_{i11}}}$
AcAc → Acetone	$r_{12} = \gamma \cdot [Adc] \cdot \frac{V_{12}[AcAc_i]}{K_{m12} + [AcAc_i]}$
AcCoA + NADH → AcAld + NAD^+	$r_{13}^a = \gamma \cdot [AdhE_1] \cdot \frac{V_{13}[AcCoA_i]}{K_{m13} + [AcCoA_i]} \cdot \frac{\frac{[NADH]}{K_{r13}^a}}{1 + \frac{[NADH]}{K_{r13}^a} + \frac{[NADPH]}{K_{r13}^b}}$
AcCoA + NADPH → AcAld + $NADP^+$	$r_{13}^b = \gamma \cdot [AdhE_1] \cdot \frac{V_{13}[AcCoA_i]}{K_{m13} + [AcCoA_i]} \cdot \frac{\frac{[NADPH]}{K_{r13}^b}}{1 + \frac{[NADH]}{K_{r13}^a} + \frac{[NADPH]}{K_{r13}^b}}$
AcAld + NADH → Ethanol + NAD^+	$r_{14}^a = \gamma \cdot [AdhE_1] \cdot \frac{V_{14}[AcAld_i]}{K_{m14} + [AcAld_i]} \cdot \frac{\frac{[NADH]}{K_{r14}^a}}{1 + \frac{[NADH]}{K_{r14}^a} + \frac{[NADPH]}{K_{r14}^b}}$
AcAld + NADPH → Ethanol + $NADP^+$	$r_{14}^b = \gamma \cdot [AdhE_1] \cdot \frac{V_{14}[AcAld_i]}{K_{m14} + [AcAld_i]} \cdot \frac{\frac{[NADPH]}{K_{r14}^b}}{1 + \frac{[NADH]}{K_{r14}^a} + \frac{[NADPH]}{K_{r14}^b}}$
AcCoA + NADH → AcAld + NAD^+	$r_{15}^a = \gamma \cdot [AdhE_2] \cdot \frac{V_{15}[AcCoA_i]}{K_{m15} + [AcCoA_i]} \cdot \frac{\frac{[NADH]}{K_{r15}^a}}{1 + \frac{[NADH]}{K_{r15}^a} + \frac{[NADPH]}{K_{r15}^b}}$
AcCoA + NADPH → AcAld + $NADP^+$	$r_{15}^b = \gamma \cdot [AdhE_2] \cdot \frac{V_{15}[AcCoA_i]}{K_{m15} + [AcCoA_i]} \cdot \frac{\frac{[NADPH]}{K_{r15}^b}}{1 + \frac{[NADH]}{K_{r15}^a} + \frac{[NADPH]}{K_{r15}^b}}$
AcAld + NADH → Ethanol + NAD^+	$r_{16}^a = \gamma \cdot [AdhE_2] \cdot \frac{V_{16}[AcAld_i]}{K_{m16} + [AcAld_i]} \cdot \frac{\frac{[NADH]}{K_{r16}^a}}{1 + \frac{[NADH]}{K_{r16}^a} + \frac{[NADPH]}{K_{r16}^b}}$
AcAld + NADPH → Ethanol + $NADP^+$	$r_{16}^b = \gamma \cdot [AdhE_2] \cdot \frac{V_{16}[AcAld_i]}{K_{m16} + [AcAld_i]} \cdot \frac{\frac{[NADPH]}{K_{r16}^b}}{1 + \frac{[NADH]}{K_{r16}^a} + \frac{[NADPH]}{K_{r16}^b}}$
AcAcCoA + NADH → 3HBCoA + NAD^+	$r_{17} = \gamma \cdot [Hbd] \cdot \frac{V_{17}[AcAcCoA_i]}{K_{m17} + [AcAcCoA_i]} \cdot \frac{[NADH]}{K_{r17} + [NADH]}$

3HBCoA → CroCoA	$r_{18} = \gamma \cdot [Crt] \cdot \frac{V_{18}[3HBCoA_i]}{K_{m18} + [3HBCoA_i]}$
CroCoA + NADH → BuCoA + NAD^+	$r_{19} = \gamma \cdot [Bcd] \cdot \frac{V_{19}[CroCoA_i]}{K_{m19} + [CroCoA_i]} \cdot \frac{[NADH]}{K_{r19} + [NADH]}$
BuCoA → BuP	$r_{20} = \gamma \cdot [Ptb] \cdot \frac{V_{20}[BuCoA_i]}{K_{m20} + [BuCoA_i]}$
BuP → BuCoA	$r_{21} = \gamma \cdot [Ptb] \cdot \frac{V_{21}[BuP_i]}{K_{m21} + [BuP_i]}$
BuP + ADP → Butyrate + ATP	$r_{22} = \gamma \cdot [Buk] \cdot \frac{V_{22}[BuP_i]}{K_{m22} + [BuP_i]} \cdot \frac{[ADP]}{K_{e22} + [ADP]}$
Butyrate + ATP → BuP + ADP	$r_{23} = \gamma \cdot [Buk] \cdot \frac{V_{23}[Butyrate_i^t]}{K_{m23} + [Butyrate_i^t]} \cdot \frac{[ATP]}{K_{e23} + [ATP]}$
Butyrate + AcAcCoA → BuCoA + AcAc	$r_{24} = \gamma \cdot [CtfAB] \cdot \frac{V_{24}}{1 + \frac{K_{m24a}}{[Butyrate_i^t]} + \frac{K_{m24b}}{[AcAcCoA_i]}} \cdot \frac{1}{1 + \frac{[AcAc_i]}{K_{i24}}}$
BuCoA + NADH → BuAld + NAD^+	$r_{25}^a = \gamma \cdot [AdhE_1] \cdot \frac{V_{25}[BuCoA_i]}{K_{m25} + [BuCoA_i]} \cdot \frac{\frac{[NADH]}{K_{r25}^a}}{1 + \frac{[NADH]}{K_{r25}^a} + \frac{[NADPH]}{K_{r25}^b}}$
BuCoA + NADPH → BuAld + $NADP^+$	$r_{25}^b = \gamma \cdot [AdhE_1] \cdot \frac{V_{25}[BuCoA_i]}{K_{m25} + [BuCoA_i]} \cdot \frac{\frac{[NADPH]}{K_{r25}^b}}{1 + \frac{[NADH]}{K_{r25}^a} + \frac{[NADPH]}{K_{r25}^b}}$
BuAld + NADH → Butanol + NAD^+	$r_{26}^a = \gamma \cdot [AdhE_1] \cdot \frac{V_{26}[BuAld_i]}{K_{m26} + [BuAld_i](1 + \frac{[Butanol_i]}{K_{i26}})} \cdot \frac{\frac{[NADH]}{K_{r26}^a}}{1 + \frac{[NADH]}{K_{r26}^a} + \frac{[NADPH]}{K_{r26}^b}}$
BuAld + NADPH → Butanol + $NADP^+$	$r_{26}^b = \gamma \cdot [AdhE_1] \cdot \frac{V_{26}[BuAld_i]}{K_{m26} + [BuAld_i](1 + \frac{[Butanol_i]}{K_{i26}})} \cdot \frac{\frac{[NADPH]}{K_{r26}^b}}{1 + \frac{[NADH]}{K_{r26}^a} + \frac{[NADPH]}{K_{r26}^b}}$
NAD^+ → NADH	$r_{27} = \gamma \cdot \frac{V_{27}[NAD^+]}{K_{r27} + [NAD^+]}$
NADH → NAD^+	$r_{28} = \gamma \cdot \frac{V_{28}[NADH]}{K_{r28} + [NADH]}$
$NADP^+$ → NADPH	$r_{29} = \gamma \cdot \frac{V_{29}[NADP^+]}{K_{r29} + [NADP^+]}$
NADPH → $NADP^+$	$r_{30} = \gamma \cdot \frac{V_{30}[NADPH]}{K_{r30} + [NADPH]}$
Fd^{ox} + NADH → Fd^{red} + NAD^+	$r_{31}^a = \gamma \cdot [Nfor] \cdot \frac{V_{31}[Fd^{ox}]}{K_{f31} + [Fd^{ox}]} \cdot \frac{\frac{[NADH]}{K_{r31}^a}}{1 + \frac{[NADH]}{K_{r31}^a} + \frac{[NADPH]}{K_{r31}^b}}$
Fd^{ox} + NADPH → Fd^{red} + $NADP^+$	$r_{31}^b = \gamma \cdot [Nfor] \cdot \frac{V_{31}[Fd^{ox}]}{K_{f31} + [Fd^{ox}]} \cdot \frac{\frac{[NADPH]}{K_{r31}^b}}{1 + \frac{[NADH]}{K_{r31}^a} + \frac{[NADPH]}{K_{r31}^b}}$
Fd^{red} + NAD^+ → Fd^{ox} + NADH	$r_{32}^a = \gamma \cdot [Fnr] \cdot \frac{V_{32}[Fd^{red}]}{K_{f32} + [Fd^{red}]} \cdot \frac{\frac{[NAD^+]}{K_{r32}^a}}{1 + \frac{[NAD^+]}{K_{r32}^a} + \frac{[NADP^+]}{K_{r32}^b}}$
Fd^{red} + $NADP^+$ → Fd^{ox} + NADPH	$r_{32}^b = \gamma \cdot [Fnr] \cdot \frac{V_{32}[Fd^{red}]}{K_{f32} + [Fd^{red}]} \cdot \frac{\frac{[NADP^+]}{K_{r32}^b}}{1 + \frac{[NAD^+]}{K_{r32}^a} + \frac{[NADP^+]}{K_{r32}^b}}$
Fd^{red} → Fd^{ox} + H_2	$r_{33} = \gamma \cdot [Hyd] \cdot \frac{V_{33}[Fd^{red}]}{K_{f33} + [Fd^{red}]}$

Table S9: Kinetic laws of the primary metabolic reactions described in Fig. S12. The kinetic rates are extended to multi-substrate enzymatic reactions according to Sec. 3.1.

6 Supplementary Figures

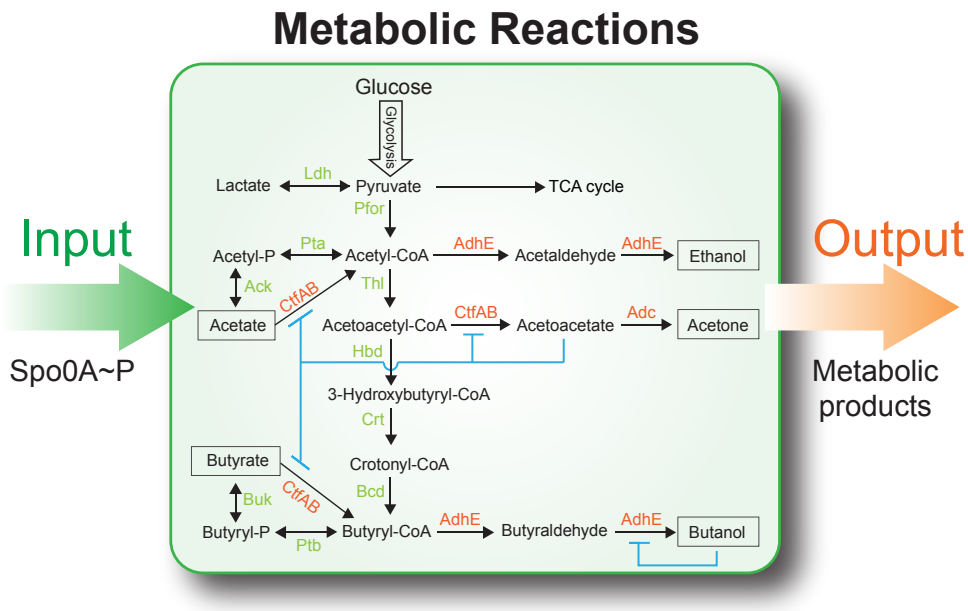

Figure S1: The detailed metabolic network for the ABE fermentation. Glucose is converted via multiple steps into acetate and butyrate (organic acids) which are re-assimilated later to synthesize acetone, butanol and ethanol (solvents). Here, the enzymes involved in acid production are constitutively expressed (green) while those in solvent synthesis are induced by the phosphorylated Spo0A (Spo0A∼P) (red). Black arrows indicate metabolic fluxes while blue flat-headed lines reflect internal production inhibitions. In this module, the concentration of Spo0A∼P serves as the input and the levels of metabolites are the output. Enzyme abbreviations: Ack, acetate kinase; Adc, acetoacetate decarboxylase; AdhE, aldehyde/alcohol dehyrogenase; Bcd, butyryl-CoA dehydrogenase; Buk, butyrate kinase; Crt, crotonase; CtfAB, acetoacetyl-CoA:acyl-CoA transferase; Hbd, 3-hydroxybutyryl-CoA dehydrogenase; Ldh, lactate dehydrogenase; Pfor, pyruvate:ferredoxin oxidoreductase; Pta, phosphotransacetylase; Ptb, phosphotransbutyrylase; and Thl, thiolase. TCA cycle stands for tricarboxylic acid cycle.

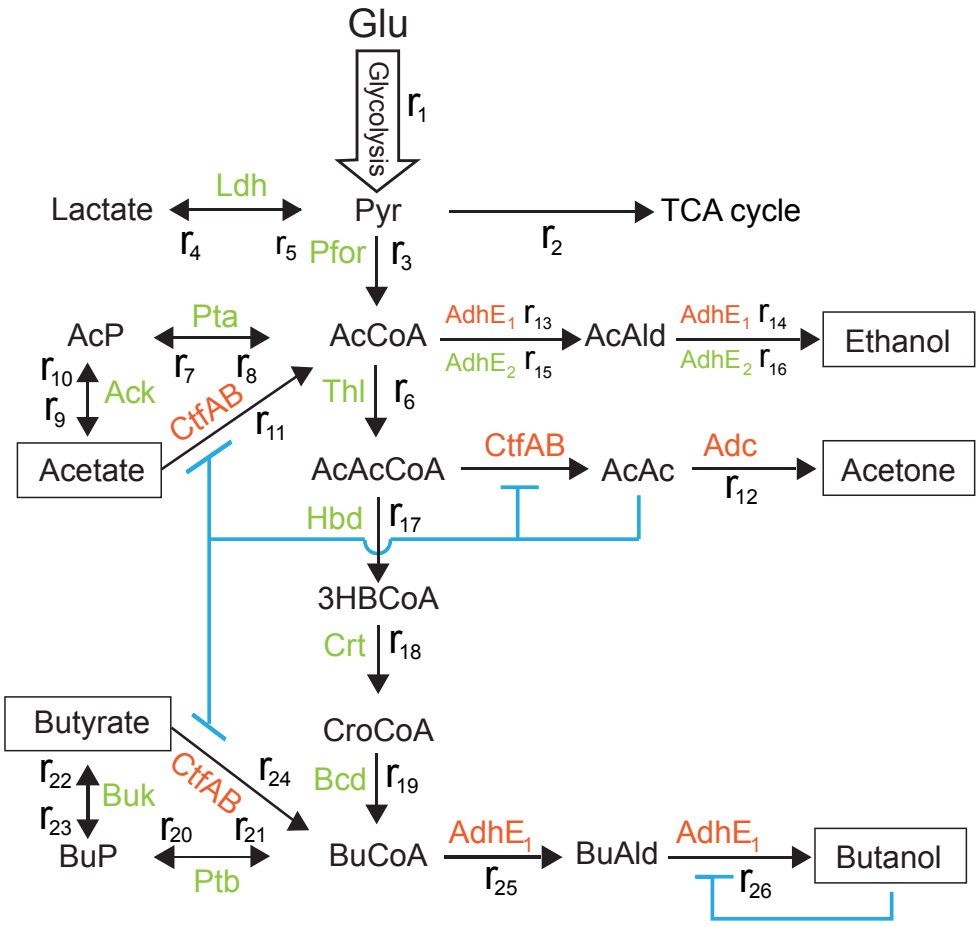

Figure S2: The pathway involves a total of 26 biochemical reactions indexed from r_1 to r_{26}. For each of the reactions, there is an associated enzyme that belongs to one of the two categories: (i) Enzymes that are constitutively expressed (green) or (ii) Enzymes controlled by Spo0A∼P (red). Additionally, there exist product inhibitions, indicated by blue flat-headed arrows. Enzyme abbreviations: Ack, acetate kinase; Adc, acetoacetate decarboxylase; AdhE, aldehyde/alcohol dehyrogenase; Bcd, butyryl-CoA dehydrogenase; Buk, butyrate kinase; Crt, crotonase; CtfAB, acetoacetyl-CoA:acyl-CoA transferase; Hbd, 3-hydroxybutyryl-CoA dehydrogenase; Ldh, lactate dehydrogenase; Pfor, pyruvate:ferredoxin oxidoreductase; Pta, phosphotransacetylase; Ptb, phosphotransbutyrylase; and Thl, thiolase. Metabolites: *Glu*, Glucose; *Pyr*, Pyruvate; *AcP*, Acetyl phosphate; *AcCoA*, Acetyl-CoA; *AcAld*, Acetaldehyde; *AcAcCoA*, Acetoacetyl-CoA; *AcAc*, Acetoacetate; *3HBCoA*, 3-Hydroxybutyryl-CoA; *CroCoA*, Crotonyl-CoA; *BuCoA*, Butyryl-CoA; *BuP*, Butyryl phosphate; *BuAld*, Butyraldehyde. TCA cycle stands for tricarboxylic acid cycle.

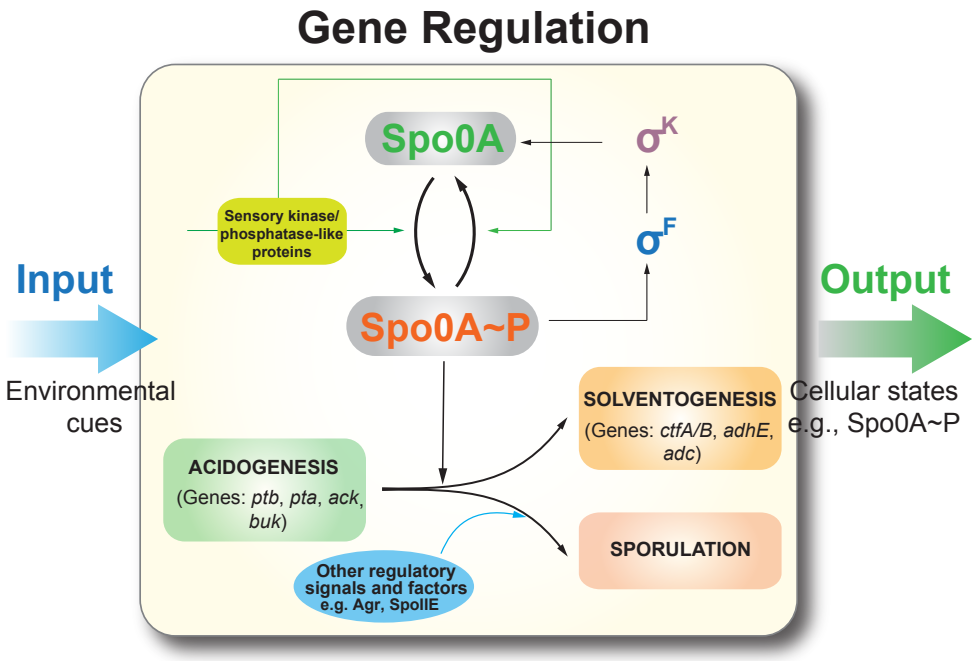

Figure S3: The core genetic controlling network. The module centers on the master regulator Spo0A and its phosphorylated form Spo0A∼P which controls cellular phase shift from acidogenesis to solventogenesis. The transitions between the two forms of Spo0A are induced by environmental signals and also regulated by double positive feedback via sigma factor F (σ^F) and sigma factor K (σ^K). In this module, the state of environmental cues, defined as cell toxicity, serves as the input and the concentration of Spo0A∼P is the output.

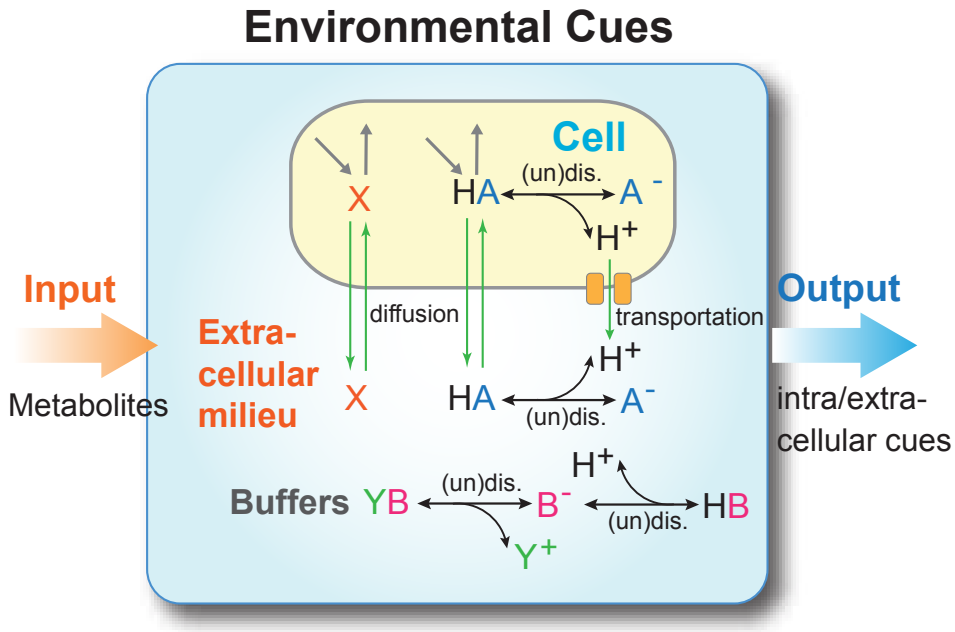

Figure S4: Schematic illustration of the processes involved in the environmental cues, including acid dissociation, metabolite diffusion, and equilibrium of protons and other ions. In this module, the system inputs are the metabolites produced by the cells and the output is the total effect of intra- and extra-cellular environmental cues which can be described by a quantitative metric, cell toxicity. (Un)dis. stands for bi-directional association and dissociation processes.

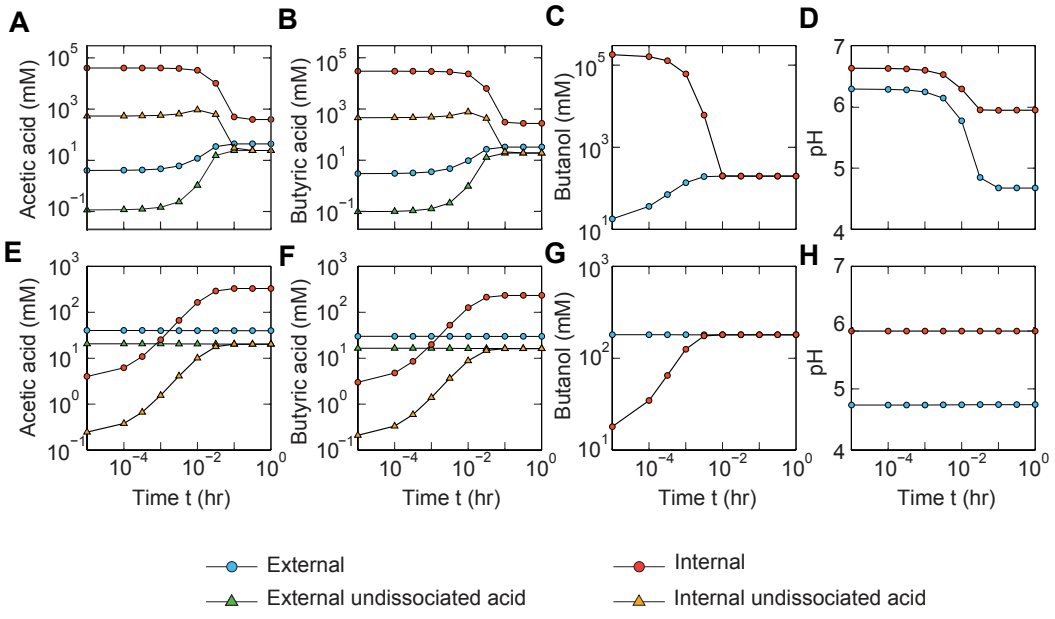

Figure S5: Equilibriums of dissociable acids and other metabolites in different initial conditions. (A-D) Initial conditions: acetic acid (intracellular 4×10^4 mM; extracellular 4 mM), butyric acid (intracellular 3×10^4 mM; extracellular 3 mM) and butanol (intracellular 1.8×10^5 mM; extracellular 18 mM). (E-H) Initial conditions: acetic acid (intracellular 4 mM; extracellular 40 mM), butyric acid (intracellular 3 mM; extracellular 30 mM) and butanol (intracellular 18 mM; extracellular 180 mM). V_r is 1.0×10^{-3}. We used MS-MES medium for pH calculation.

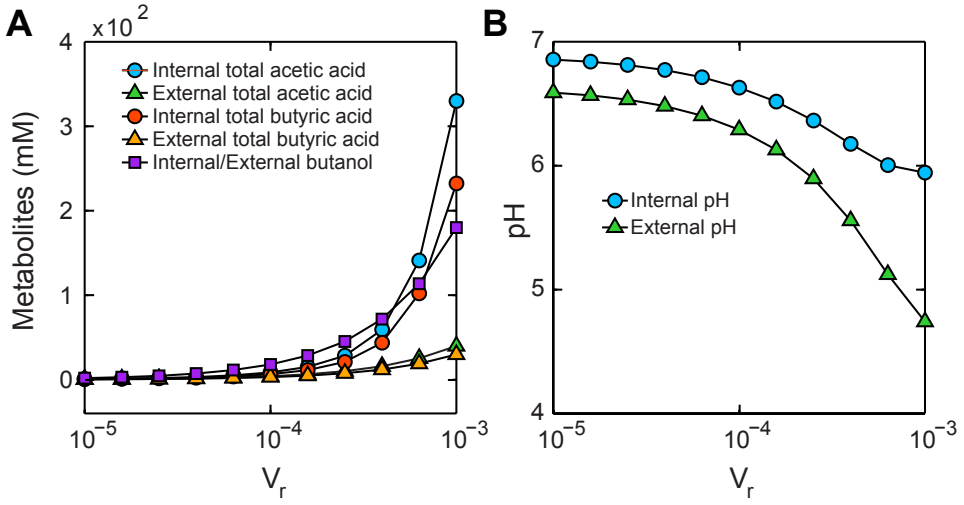

Figure S6: The impacts of cell density on metabolite equilibrium and pH. Initial conditions: acetic acid (intracellular 4×10^4 mM; extracellular 4 mM), butyric acid (intracellular 3×10^4 mM; extracellular 3 mM) and butanol (intracellular 1.8×10^5 mM; extracellular 18 mM). We used MS-MES medium for pH calculation.

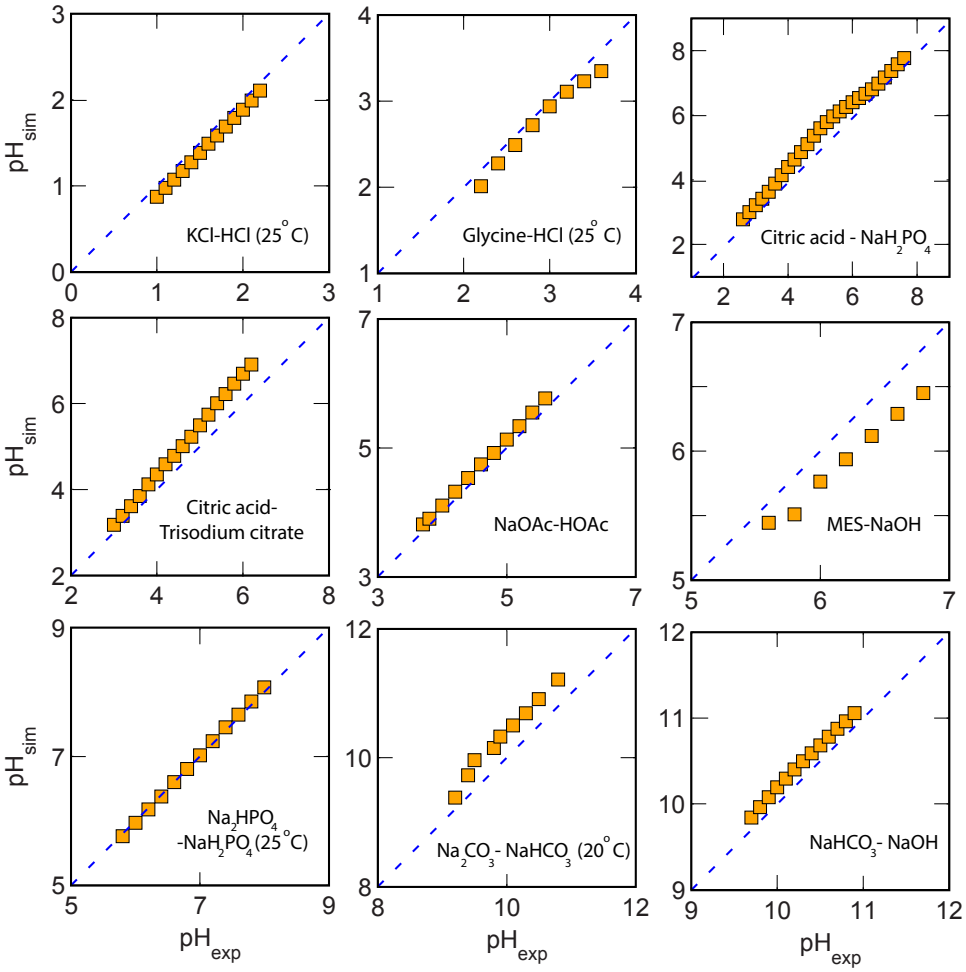

Figure S7: Validation of the charge balance approach for pH calculaion using simple buffers. The X and Y axes correspond to the experimental data (54) and numerical simulations respectively.

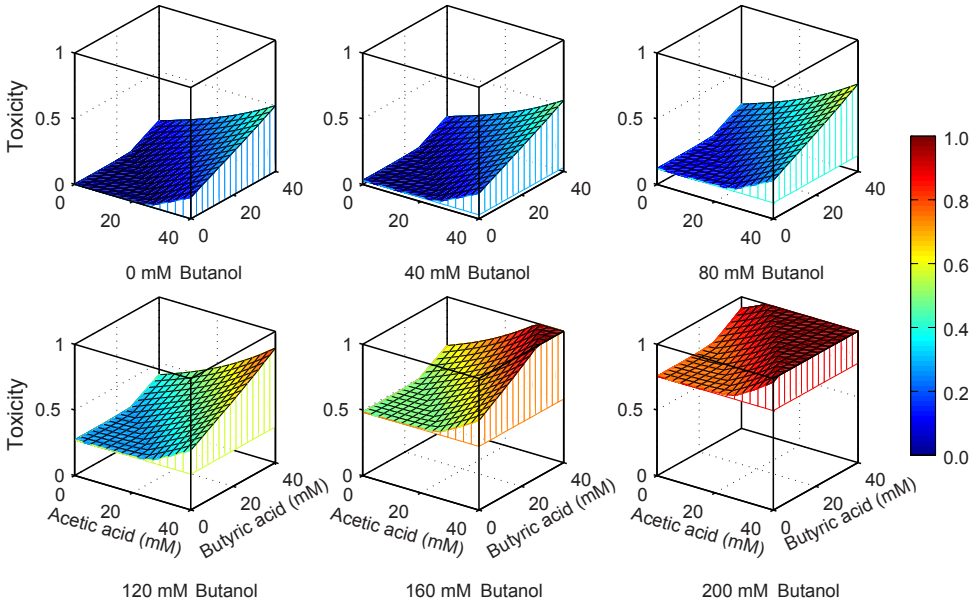

Figure S8: Cellular toxicity C_t as a function of acetic acid and butyric acid for a given level of butanol. We used MS-MES medium for pH calculation.

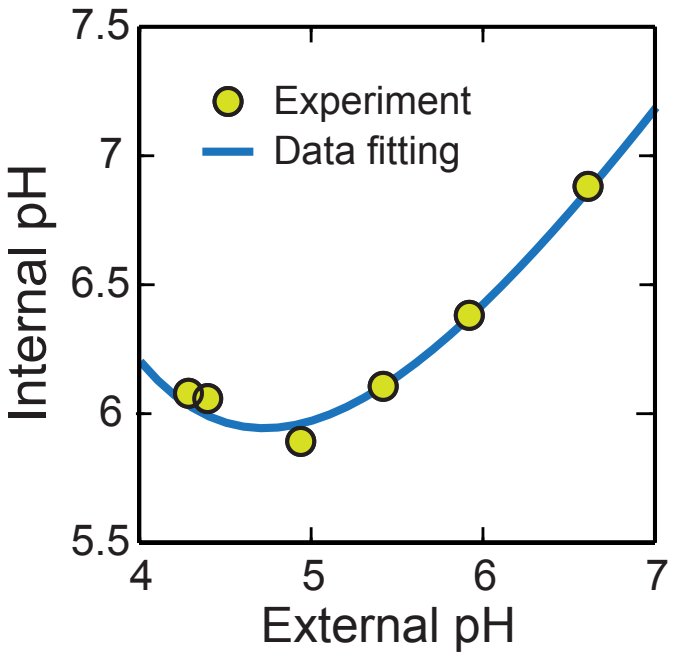

Figure S9: Comparison of the intra- and extra-cellular pH relationship from an empirical equation with that from experimental measurement (33).

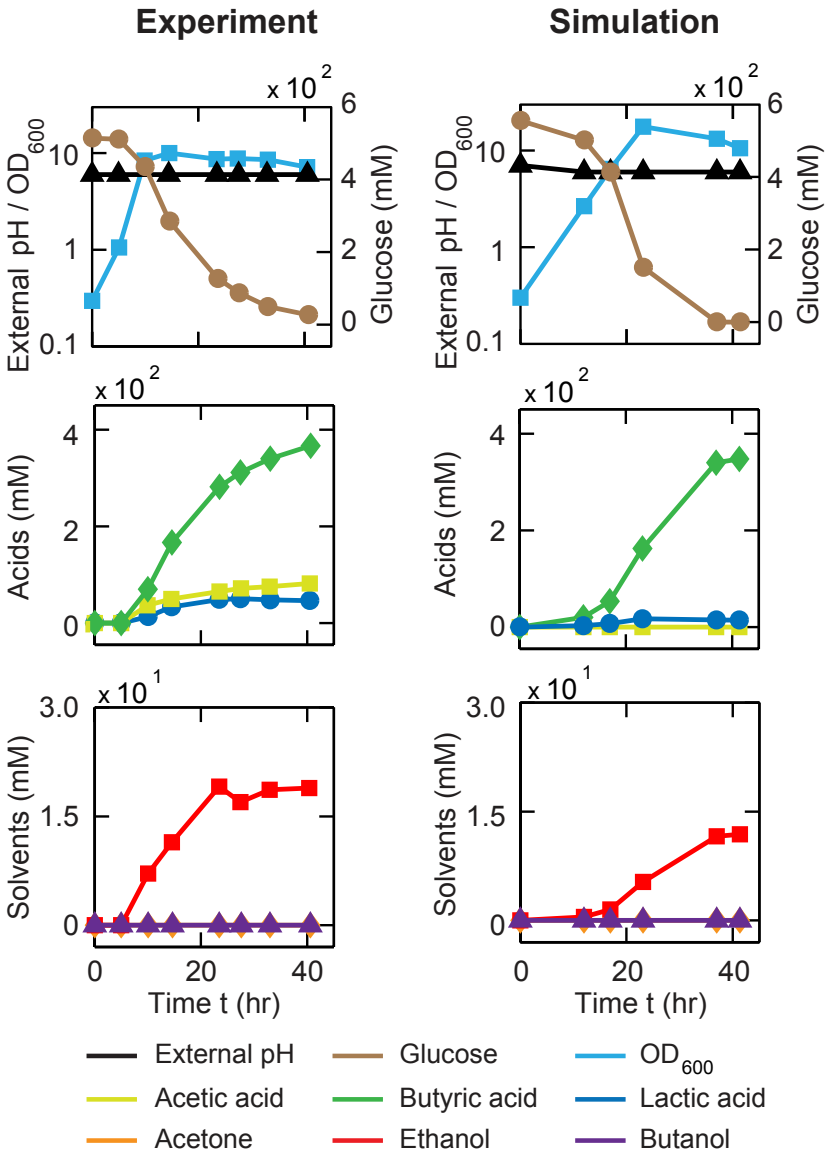

Figure S10: Comparison of the experimental and simulated metabolite profiles for a pH-controlled (pH ≥ 6.0) batch fermentation. A *pta-ctfB-adhE*$_1$ triple-knockout strain was used (8).

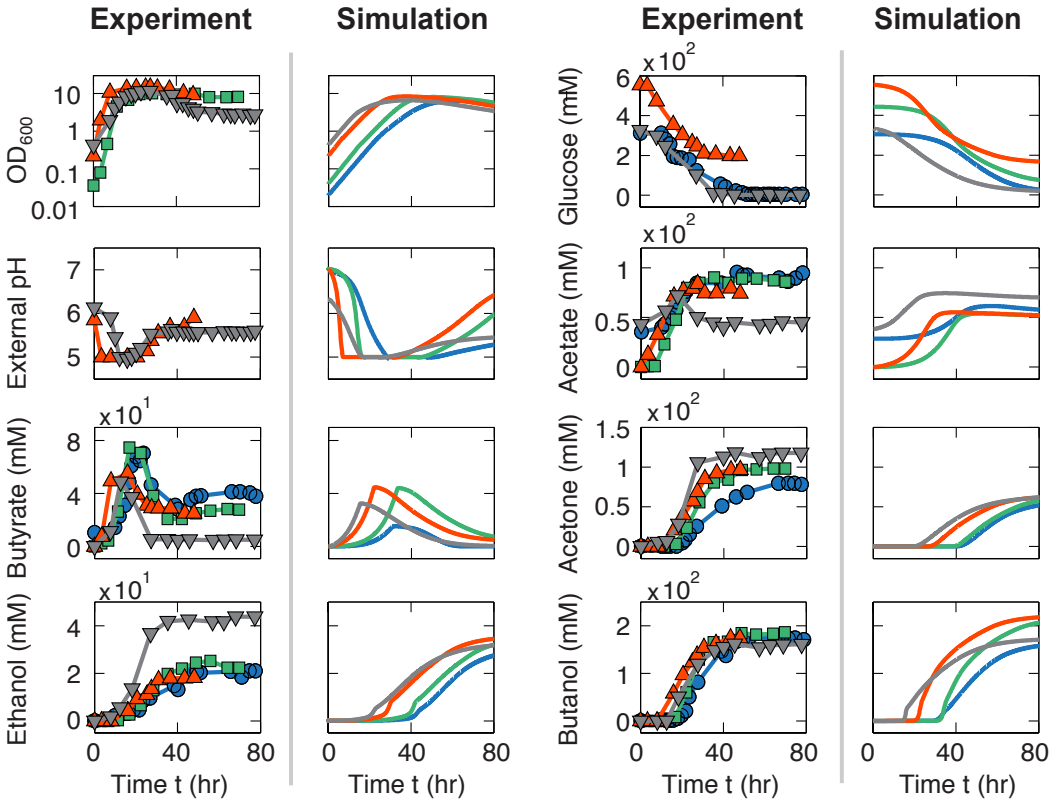

Figure S11: Comparison of experimental and simulated metabolite profiles for multiple pH-controlled ($\text{pH} \geq 5.0$) batch fermentations. The same wild-type strain was used, however, media and initial glucose levels were different. Data sources: blue circles (52), red triangles (53), green squares (19), gray inverted triangles (2).

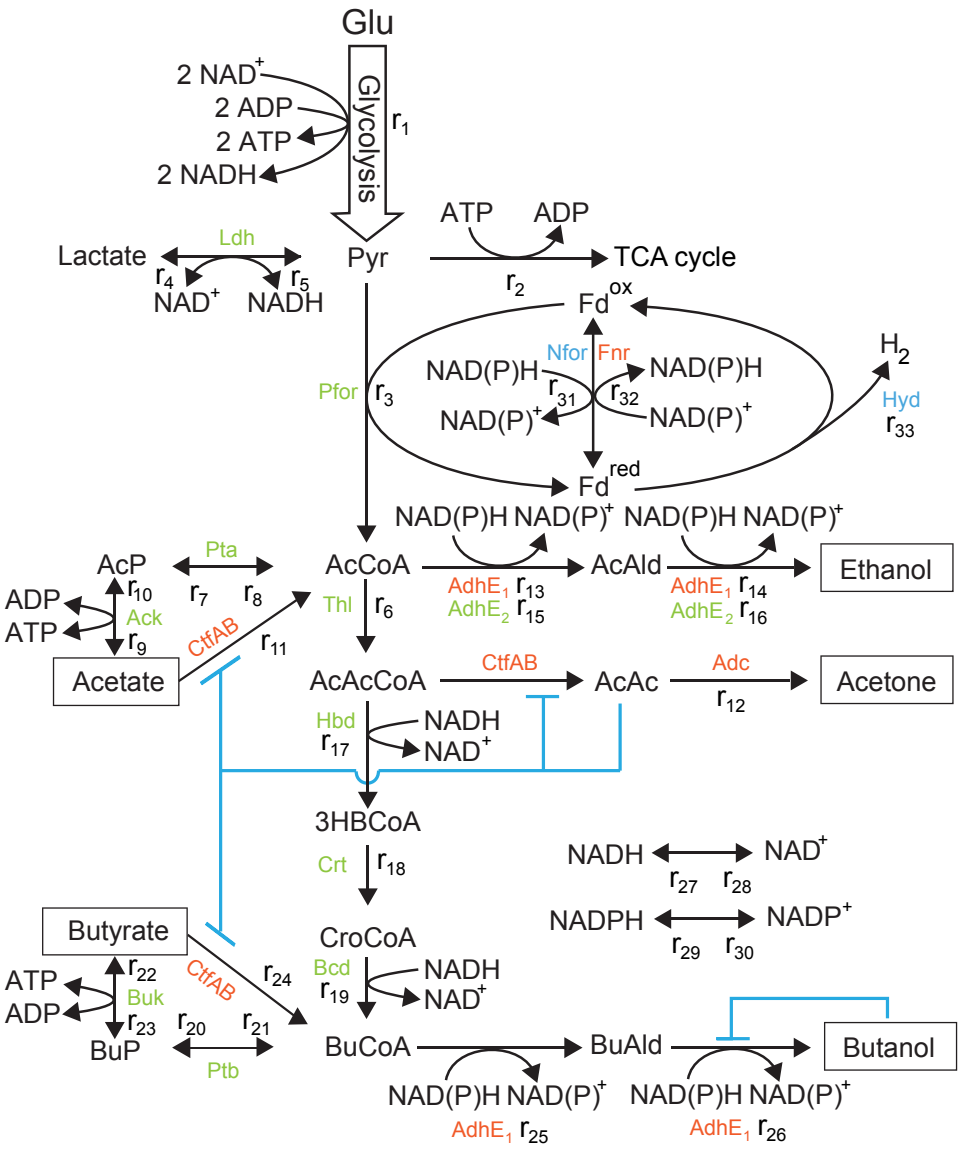

Figure S12: The pathway involves a total of 33 biochemical reactions indexed from r_1 to r_{33}. For each of the reactions, there is an associated enzyme that belongs to one of the three categories: (i) Enzymes that are constitutively expressed (green); (ii) Enzymes that are up-regulated in solventogenesis (red); (iii) Enzymes that are down-regulated in solventogenesis (blue). Additionally, there exist product inhibitions, indicated by blue flat-headed arrows. Enzymes: Ldh, lactate dehydrogenase; Pfor, pyruvate:ferredoxin oxidoreductase; Nfor, NAD(P)H-ferredoxin oxidoreductase; Fnr, ferredoxin-NAD(P)$^+$ reductase; Hyd, hydrogenase; Pta, phosphotransacetylase; Ack, acetate kinase; AdhE, aldehyde/alcohol dehyrogenase; CtfAB, acetoacetyl-CoA:acyl-CoA transferase; Adc, acetoacetate decarboxylase; Thl, thiolase; Hbd, 3-hydroxybutyryl-CoA dehydrogenase; Crt, crotonase; Bcd, butyryl-CoA dehydrogenase; Ptb, phosphotransbutyrylase; Buk, butyrate kinase. Metabolites: *Glu*, Glucose; *Pyr*, Pyruvate; *AcP*, Acetyl phosphate; *AcCoA*, Acetyl-CoA; *AcAld*, Acetaldehyde; *AcAcCoA*, Acetoacetyl-CoA; *AcAc*, Acetoacetate; *3HBCoA*, 3-Hydroxybutyryl-CoA; *CroCoA*, Crotonyl-CoA; *BuCoA*, Butyryl-CoA; *BuP*, Butyryl phosphate; *BuAld*, Butyraldehyde; *ATP*, Adenosine triphosphate; *ADP*, Adenosine diphosphate; *NADH/NAD*$^+$, Nicotinamide adenine dinucleotide; *NADPH/NADP*$^+$, Nicotinamide adenine dinucleotide phosphate. Others: Fd^{ox}/Fd^{red}, oxidized/reduced ferredoxin; H_2, hydrogen. TCA cycle stands for tricarboxylic acid cycle.

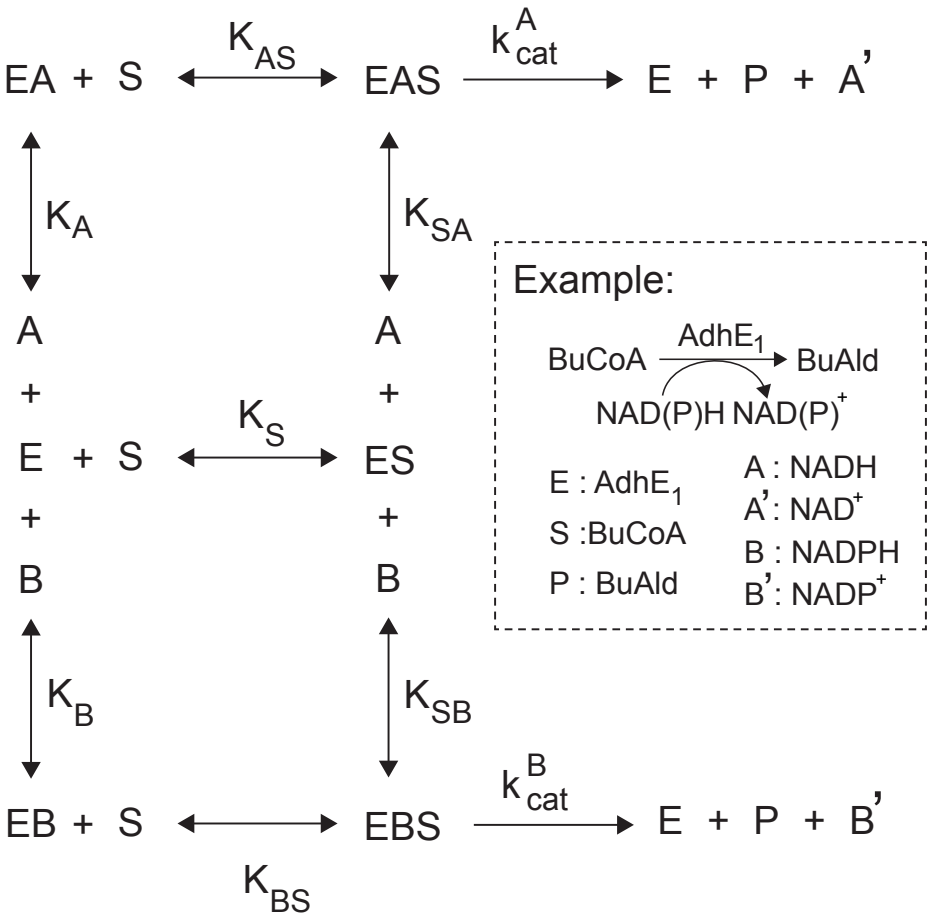

Figure S13: Random tri-substrate mechanism of enzymatic reactions. The conversion from substrate S to product P is mediated by the enzyme E with two alternative cofactors A and B, which are converted to A' and B' correspondingly. The substrate and cofactors bind to the enzyme randomly and the reaction takes place only after the enzyme is bound to both. The dissociation constant is given for each reversible reaction.

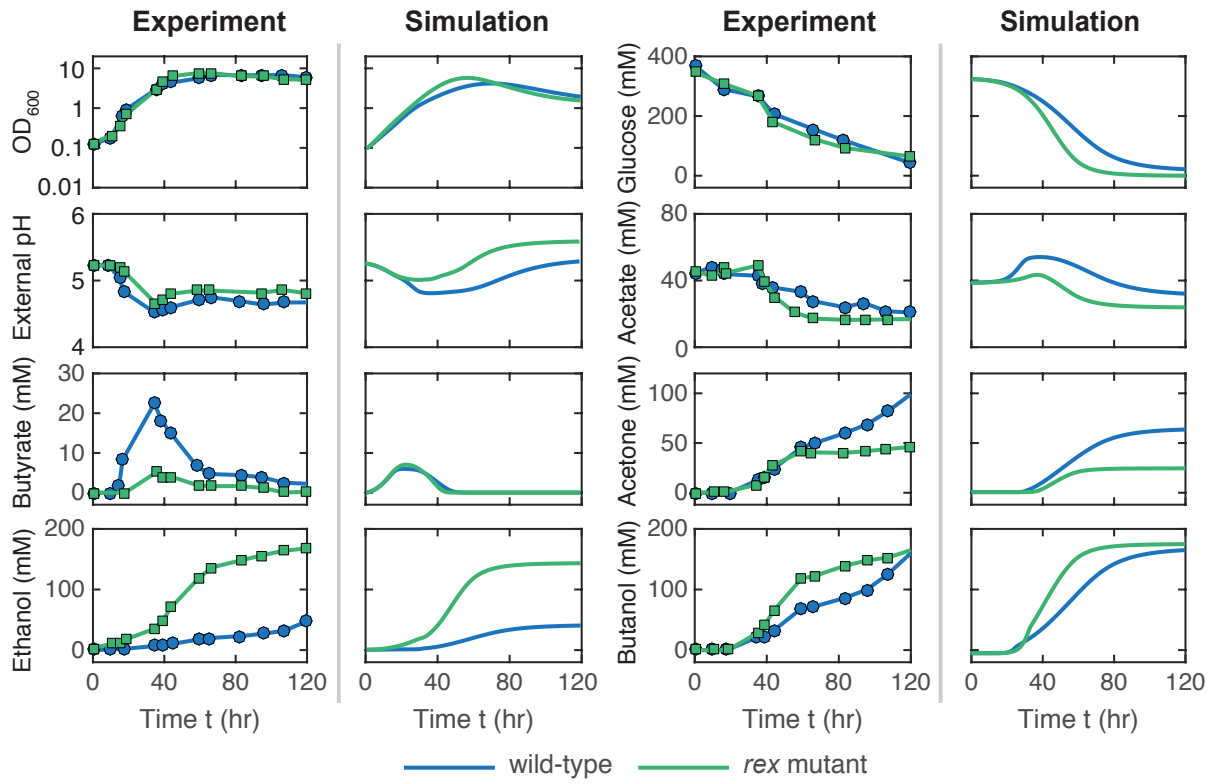

Figure S14: Comparison of the experimental and simulated metabolite profiles for a pH-uncontrolled batch fermentation of both the wild-type strain and a *rex* mutant (45).

7 Supplemental References

1. Amador-Noguez D, Brasg IA, Feng XJ, Roquet N, Rabinowitz JD (2011) Metabolome remodeling during the acidogenic-solventogenic transition in *Clostridium acetobutylicum*. *Appl Environ Microbiol* 77(22):7984–7997.

2. Lehmann D, Radomski N, Lütke-Eversloh T (2012) New insights into the butyric acid metabolism of *Clostridium acetobutylicum*. *Appl Microbiol Biotechnol* 96(5):1325–1339.

3. Shinto H, et al. (2007) Kinetic modeling and sensitivity analysis of acetone–butanol–ethanol production. *J Biotechnol* 131(1):45–56.

4. Gheshlaghi R, Scharer JM, Moo-Young M, Chou CP (2009) Metabolic pathways of clostridia for producing butanol. *Biotechnol Adv* 27(6):764–781.

5. Wiesenborn DP, Rudolph F, Papoutsakis E (1989) Coenzyme a transferase from *Clostridium acetobutylicum* ATCC 824 and its role in the uptake of acids. *Appl Environ Microbiol* 55(2):323–329.

6. Grimmler C, et al. (2011) Genome-wide gene expression analysis of the switch between acidogenesis and solventogenesis in continuous cultures of *Clostridium acetobutylicum*. *J Mol Microbiol Biotechnol* 20(1):1–15.

7. Jang YS, Im JA, Choi SY, Lee JI, Lee SY (2014) Metabolic engineering of *Clostridium acetobutylicum* for butyric acid production with high butyric acid selectivity. *Metab Eng* 23(0):165–174.

8. Jang YS, Woo HM, Im JA, Kim IH, Lee SY (2013) Metabolic engineering of *Clostridium acetobutylicum* for enhanced production of butyric acid. *Appl Microbiol Biotechnol* 97(21):9355–9363.

9. Lee SY, et al. (2008) Fermentative butanol production by clostridia. *Biotechnol Bioeng* 101(2):209–228.

10. Hartmanis MG, Gatenbeck S (1984) Intermediary metabolism in *Clostridium acetobutylicum*: levels of enzymes involved in the formation of acetate and butyrate. *Appl Environ Microbiol* 47(6):1277–1283.

11. Monod J (1949) The growth of bacterial cultures. *Annu Rev Microbiol* 3(1):371–394.

12. Bowles LK, Ellefson WL (1985) Effects of butanol on *Clostridium acetobutylicum*. *Appl Environ Microbiol* 50(5):1165–1170.

13. Yang X, Tsao GT (1994) Mathematical modeling of inhibition kinetics in acetone-butanol fermentation by *Clostridium acetobutylicum*. *Biotechnol Prog* 10(5):532–538.

14. Cooksley CM, et al. (2012) Targeted mutagenesis of the *Clostridium acetobutylicum* acetone–butanol–ethanol fermentation pathway. *Metab Eng* 14(6):630–641.

15. Kovárová-Kovar K, Egli T (1998) Growth kinetics of suspended microbial cells: from single-substrate-controlled growth to mixed-substrate kinetics. *Microbiol Mol Biol Rev* 62(3):646–666.

16. Pirt S (1982) Maintenance energy: a general model for energy-limited and energy-sufficient growth. *Arch Microbiol* 133(4):300–302.

17. Van Bodegom P (2007) Microbial maintenance: a critical review on its quantification. *Microb Ecol* 53(4):513–523.

18. Paredes CJ, Alsaker KV, Papoutsakis ET (2005) A comparative genomic view of clostridial sporulation and physiology. *Nat Rev Microbiol* 3(12):969–978.

19. Harris LM, Welker NE, Papoutsakis ET (2002) Northern, morphological, and fermentation analysis of *spo0A* inactivation and overexpression in *Clostridium acetobutylicum* ATCC 824. *J Bacteriol* 184(13):3586–3597.

20. Al-Hinai M, Jones S, Papoutsakis E (2014) σ^{k} of *Clostridium acetobutylicum* is the first known sporulation-specific sigma factor with two developmentally separated roles, one early and one late in sporulation. *J Bacteriol* 196(2):287–299.

21. Al-Hinai M, Jones S, Papoutsakis E (2015) The *Clostridium* sporulation programs: Diversity and preservation of endospore differentiation. *Microbiol Mol Biol Rev* 79(1):19–37.

22. Gottwald M, Gottschalk G (1985) The internal pH of *Clostridium acetobutylicum* and its effect on the shift from acid to solvent formation. *Arch Microbiol* 143(1):42–46.

23. Maddox I, et al. (2000) The cause of "acid crash" and "acidogenic fermentations" during the batch acetone-butanol-ethanol (ABE-) fermentation process. *J Mol Microbiol Biotechnol* 2(1):95–100.

24. Zhao Y, Tomas CA, Rudolph FB, Papoutsakis ET, Bennett GN (2005) Intracellular butyryl phosphate and acetyl phosphate concentrations in *Clostridium acetobutylicum* and their implications for solvent formation. *Appl Environ Microbiol* 71(1):530–537.

25. Alsaker KV, Paredes C, Papoutsakis ET (2010) Metabolite stress and tolerance in the production of biofuels and chemicals: Gene-expression-based systems analysis of butanol, butyrate, and acetate stresses in the anaerobe *Clostridium acetobutylicum*. *Biotechnol Bioeng* 105(6):1131–1147.

26. Cho DH, Shin SJ, Kim YH (2012) Effects of acetic and formic acid on ABE production by *Clostridium acetobutylicum* and *Clostridium beijerinckii*. *Biotechnol Bioprocess Eng* 17(2):270–275.

27. Vázquez JA, et al. (2011) Evaluation of toxic effects of several carboxylic acids on bacterial growth by toxicodynamic modelling. *Microb Cell Fact* 10:100.

28. Baronofsky JJ, Schreurs WJ, Kashket ER (1984) Uncoupling by acetic acid limits growth of and acetogenesis by *Clostridium thermoaceticum*. *Appl Environ Microbiol* 48(6):1134–1139.

29. Jones DT, Woods DR (1986) Acetone-butanol fermentation revisited. *Microbiol Rev* 50(4):484.

30. Dougherty DP, Da Conceicao Neta ER, McFeeters RF, Lubkin SR, Breidt F (2006) Semi-mechanistic partial buffer approach to modeling pH, the buffer properties, and the distribution of ionic species in complex solutions. *J Agric Food Chem* 54(16):6021–6029.

31. Senger RS, Papoutsakis ET (2008) Genome-scale model for *Clostridium acetobutylicum*: Part II. Development of specific proton flux states and numerically determined sub-systems. *Biotechnol Bioeng* 101(5):1053–1071.

32. Lehmann D, et al. (2012) Modifying the product pattern of *Clostridium acetobutylicum*. *Appl Microbiol Biotechnol* 94(3):743–754.

33. Huang L, Gibbins LN, Forsberg CW (1985) Transmembrane pH gradient and membrane potential in *Clostridium acetobutylicum* during growth under acetogenic and solventogenic conditions. *Appl Environ Microbiol* 50(4):1043–1047.

34. Terracciano JS, Kashket ER (1986) Intracellular conditions required for initiation of solvent production by *Clostridium acetobutylicum*. *Appl Environ Microbiol* 52(1):86–91.

35. Tracy BP, Gaida SM, Papoutsakis ET (2008) Development and application of flow-cytometric techniques for analyzing and sorting endospore-forming clostridia. *Appl Environ Microbiol* 74(24):7497–7506.

36. Jabbari S, Heap JT, King JR (2011) Mathematical modelling of the sporulation-initiation network in *Bacillus subtilis* revealing the dual role of the putative quorum-sensing signal molecule PhrA. *Bull Math Biol* 73(1):181–211.

37. Grupe H, Gottschalk G (1992) Physiological events in *Clostridium acetobutylicum* during the shift from acidogenesis to solventogenesis in continuous culture and presentation of a model for shift induction. *Appl Environ Microbiol* 58(12):3896–3902.

38. Cintolesi A, Clomburg J, Rigou V, Zygourakis K, Gonzalez R (2012) Quantitative analysis of the fermentative metabolism of glycerol in *Escherichia coli*. *Biotechnol Bioeng* 109(1):187–198.

39. Kadir T, Mannan A, Kierzek A, McFadden J, Shimizu K (2010) Modeling and simulation of the main metabolism in *Escherichia coli* and its several single-gene knockout mutants with experimental verification. *Microb Cell Fact* 9:88.

40. Parachin N, Bergdahl B, van Niel E, Gorwa-Grauslund M (2011) Kinetic modelling reveals current limitations in the production of ethanol from xylose by recombinant *Saccharomyces cerevisiae*. *Metab Eng* 13(5):508–517.

41. Berríoís-Rivera S, Bennett G, San K (2002) Metabolic engineering of *Escherichia coli*: increase of NADH availability by overexpressing an NAD^+-dependent formate dehydrogenase. *Metab Eng* 4(3):217–229.

42. Cook P, Cleland W (2007) *Enzyme kinetics and mechanism* (Garland Science).

43. Klipp E, Nordlander B, Krüger R, Gennemark P, Hohmann S (2005) Integrative model of the response of yeast to osmotic shock. *Nat Biotechnol* 23(8):975–982.

44. Marczak R, Ballongue J, Petitdemange H, Gay R (1985) Differential levels of ferredoxin and rubredoxin in *Clostridium acetobutylicum*. *Biochimie* 67(2):241–248.

45. Wietzke M, Bahl H (2012) The redox-sensing protein Rex, a transcriptional regulator of solventogenesis in *Clostridium acetobutylicum*. *Appl Microbiol Biotechnol* 96(3):749–761.

46. Zhang L, et al. (2014) Redox-responsive repressor Rex modulates alcohol production and oxidative stress tolerance in *Clostridium acetobutylicum*. *J Bacteriol* 196(22):3949–3963.

47. Wrba A, Jaenicke R, Robert H, Stetter KO (1990) Lactate dehydrogenase from the extreme thermophile *Thermotoga maritima*. *Eur J Biochem* 188(1):195–201.

48. Thorn GJ, King JR, Jabbari S (2013) pH-induced gene regulation of solvent production by *Clostridium acetobutylicum* in continuous culture: Parameter estimation and sporulation modelling. *Math Biosci* 241(2):149–166.

49. Lehmann D, Lütke-Eversloh T (2011) Switching *Clostridium acetobutylicum* to an ethanol producer by disruption of the butyrate/butanol fermentative pathway. *Metab Eng* 13(5):464–473.

50. Tomas CA, et al. (2003) DNA array-based transcriptional analysis of asporogenous, nonsolventogenic *Clostridium acetobutylicum* strains SKO1 and M5. *J Bacteriol* 185(15):4539–4547.

51. Alsaker KV, Spitzer TR, Papoutsakis ET (2004) Transcriptional analysis of *spo0A* overexpression in *Clostridium acetobutylicum* and its effect on the cell's response to butanol stress. *J Bacteriol* 186(7):1959–1971.

52. Monot F, Engasser JM, Petitdemange H (1984) Influence of pH and undissociated butyric acid on the production of acetone and butanol in batch cultures of *Clostridium acetobutylicum*. *Appl Microbiol Biotechnol* 19(6):422–426.

53. Jang YS, et al. (2012) Enhanced butanol production obtained by reinforcing the direct butanol-forming route in *Clostridium acetobutylicum*. *MBio* 3(5):e00314–12.

54. Dawson RMC, Elliott DC, Elliott WH, Jones KM (1986) *Data for biochemical research* (Clarendon Press, Oxford).